

Review

## Recent Advances in Carbon Supported Metal Nanoparticles Preparation for Oxygen Reduction Reaction in Low Temperature Fuel Cells

Yaovi Holade, Nihat Ege Sahin, Karine Servat, Teko W. Napporn and Kouakou B. Kokoh \*

Université de Poitiers, UMR CNRS 7285, « Équipe SAMCat »; 4, rue Michel Brunet, B27, TSA 51106, 86073 Poitiers cedex 09, France; E-Mails: yaovi.holade@univ-poitiers.fr (Y.H.); nihat.ege.sahin@univ-poitiers.fr (N.E.S.); karine.servat@univ-poitiers.fr (K.S.); teko.napporn@univ-poitiers.fr (T.W.N.)

\* Author to whom correspondence should be addressed; E-Mail: boniface.kokoh@univ-poitiers.fr; Tel.: +33-549-45-41-20; Fax: +33-549-45-35-80.

Academic Editor: Minhua Shao

Received: 19 December 2014 / Accepted: 26 February 2015 / Published: 6 March 2015

---

**Abstract:** The oxygen reduction reaction (ORR) is the oldest studied and most challenging of the electrochemical reactions. Due to its sluggish kinetics, ORR became the major contemporary technological hurdle for electrochemists, as it hampers the commercialization of fuel cell (FC) technologies. Downsizing the metal particles to nanoscale introduces unexpected fundamental modifications compared to the corresponding bulk state. To address these fundamental issues, various synthetic routes have been developed in order to provide more versatile carbon-supported low platinum catalysts. Consequently, the approach of using nanocatalysts may overcome the drawbacks encountered in massive materials for energy conversion. This review paper aims at summarizing the recent important advances in carbon-supported metal nanoparticles preparation from colloidal methods (microemulsion, polyol, impregnation, Bromide Anion Exchange...) as cathode material in low temperature FCs. Special attention is devoted to the correlation of the structure of the nanoparticles and their catalytic properties. The influence of the synthesis method on the electrochemical properties of the resulting catalysts is also discussed. Emphasis on analyzing data from theoretical models to address the intrinsic and specific electrocatalytic properties, depending on the synthetic method, is incorporated throughout. The synthesis process-nanomaterials structure-catalytic activity relationships highlighted herein, provide ample new rational, convenient and

straightforward strategies and guidelines toward more effective nanomaterials design for energy conversion.

**Keywords:** electrocatalysts; oxygen reduction reaction; fuel cell; nanoparticles preparation; water in oil microemulsion; platinum; palladium

---

## 1. Introduction

Formerly, electrocatalysis was practiced with metals in the bulk state. Electrochemists became aware very early of a number of obstacles and/or limitations of fundamental and economic order. On a fundamental level, it is difficult to tune the activity and selectivity of the electrodes enabling the design of advanced energy converters. Since catalysis is a surface science [1–3], the use of a bare electrode has a huge economical impact. The recent advances in nanomaterial science enable the control of the nanoparticle growth steps for rational and effective preparation of nanostructures with different shapes and sizes. Seminal papers from different research groups have shown that the electrocatalytic properties of the metals depend quasi-exclusively on their crystallographic structures [2,4]. As electrochemical reactions involve the surface of the electrode, the bulk material is only of fundamental interest and thus serves as a model electrode for reaction testing. Concerning the oxygen reduction reaction, ORR, recently fundamental investigations have effectively and definitively demonstrated that its kinetics strongly depends on the particle size correlated with the corresponding aftermath [5–8]. Especially, Shao and coworkers unexpectedly found that the optimum particle size window for Pt is roughly 2.2 nm during ORR tests in perchloric acid, while the activity decreases drastically for ultra small particles [6].

Nanomaterials have different and unique physicochemical properties compared to the bulk metals from which they result. There are undoubtedly corollaries of their sizes and shapes. They exhibit special optical, magnetic, electronic, and catalytic properties. Consequently, they can be used in various applications either ranging from physics to chemistry or from bionanotechnology to medicine. Plainly speaking about ORR considered as the major contemporary technological hurdle, electrochemists are wondering how to reduce electrode cost without losing performance or durability and, to reduce cathode loadings under  $0.1 \text{ mg}_{\text{PGM}} \text{ cm}^{-2}$  (United States Department of Energy (DOE) 2015 & 2017 targets [9]), while keeping the same activities. The approaches mostly emerging, focus on the catalytic nanoparticles' surface structure and composition to achieve such gates (Figure 1). For this objective, new nanocatalyst preparation protocols have been introduced. Amongst these synthetic routes, featuring colloidal methods, high-surface area and conducting, carbon-based materials are employed to ultra-disperse platinum group metal (PGM) nanoparticles [10–14]. Figure 1 shows the kinetic activities of Pt-based electrocatalysts prepared from the major chemical synthetic approaches. The catalytic ability of an electrode material toward ORR is performed either by rotating disc electrode (RDE) or in membrane electrode assembly (MEA); it is currently expressed using the real electrochemical active surface (ECSA), the kinetic current density,  $j_k$ , ( $\text{mA cm}^{-2}_{\text{PGM}}$ ) or the metal content ( $\text{mA } \mu\text{g}^{-1}_{\text{PGM}}$ ) (Figure 1a). When ECSA increases,  $j_k$  decreases for the same activity expressed in  $\text{mA } \mu\text{g}^{-1}_{\text{PGM}}$ , as can be seen in Figure 1b. The DOE's 2015 target is  $0.7 \text{ mA cm}^{-2}_{\text{PGM}}$ . Currently, the

state-of-the-art commercial pure Pt/C catalysts (2–4 nm) have specific activities of 0.15–0.20 mA cm<sup>-2</sup><sub>PGM</sub> and 0.10–0.12 mA μg<sup>-1</sup><sub>PGM</sub> measured in MEAs [9].

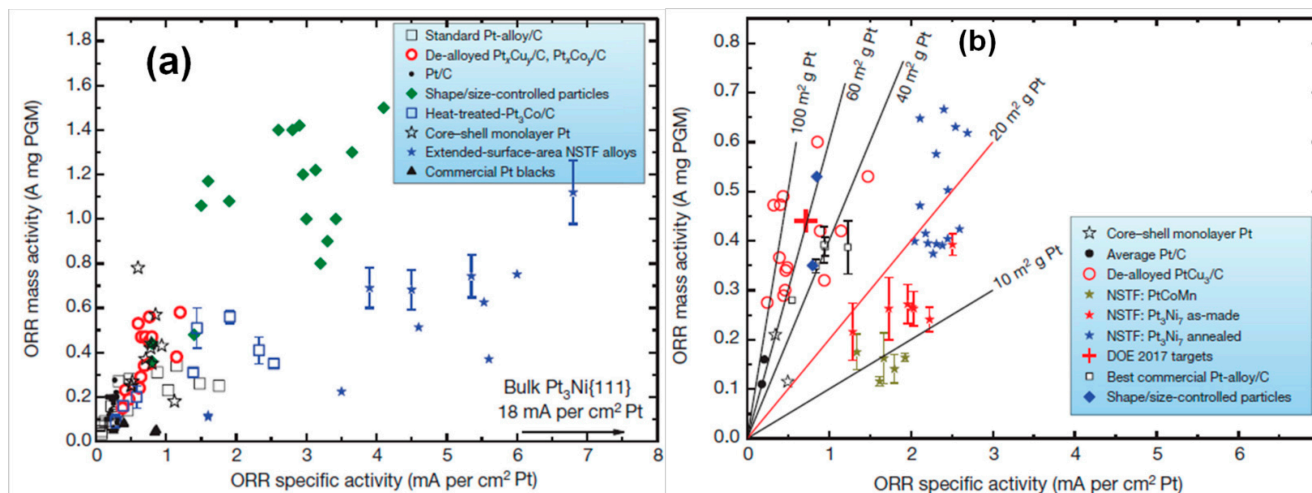


**Figure 1.** Kinetic activities of the main Pt-based electrocatalyst systems at 0.9 V vs. Reversible Hydrogen Electrode (RHE): (a) Activities are measured by rotating disc electrode (RDE) and (b) Activities are measured in membrane electrode assemblies (MEAs) at 80 °C and 150 kPa saturated O<sub>2</sub>. Reprinted with permission from Ref. [9]. Copyright 2012, Nature Publishing Group.

In gas-phase heterogeneous catalysis, the metal loading on the support typically ranges from 0.1–1 wt%. Conversely to these kind of catalysts, the metal content in the electrocatalysts must be at least 10 wt%, due to the reduced mass-transport rates of the reactant molecules in the liquid phase *versus* the gas phase [15]. The most used support material for electrocatalyst preparation is carbon black. It should be emphasized that other carbon-based materials are used as supports e.g., carbon nanotubes [16,17], single/multi-walled carbon nanotubes [18,19], buckypaper [16], carbon nanofibers [20,21]; depending on the synthesis protocols. The exceptional electrical, physical, and thermal properties of these advanced carbon-based nanocomposites make them a preferential choice in electronics [17,22], bionanotechnology [16,17,20], energy conversion and storage [17,23,24]. However, even now, carbon black powder (Vulcan XC 72 or XC 72R) is the preferred support for low temperature FCs applications. In addition to the high metal loading, its relatively inert character implies that the widespread used method in gas-phase heterogeneous catalysts preparation such as ion exchange [25] is not effective and suitable in the electrocatalyst's case. To overcome this, the electrocatalyst synthesis is based on chemical/colloidal methods. In this context, various processes have been developed. Basically, these routes can be classified into two categories: physical and chemical techniques [2,26]. The main advantage of the chemical routes is the facility of controlling and handling the primary structures of metal nanoparticles, such as size, shape and composition (in the case of multimetallic nanomaterials) as well as to achieve large-scale production. For the physical methods, all these crucial operations are more difficult.

This review aims to discuss the recent advances in the preparation of highly dispersed nanoparticles onto carbon-based substrates for low temperature FCs applications. These kinds of electrode materials enable increasing of the surface-to-volume ratio and thus the electrochemical reaction rates [5,27,28].

We focus on the recent developments regarding nanocatalysts preparation from water-in-oil microemulsion [29–34], polyol-based [35], impregnation-reduction and Bromide Anion Exchange synthetic routes [36–38].

## 2. Strategies to Synthesize Carbon Supported Nanocatalysts

### 2.1. Heterogeneous Catalysis: The Major Emergency for Supported Nanomaterials Design

Various synthetic routes have been successfully developed over the last twenty years for carbon supported nanoparticle preparation to be used in electrocatalysis, and particularly in ORR science. It is interesting to know why a support is needed during catalyst preparation. In catalysis, it is reported that the direct immobilization of metal nanoparticles onto carbon-based substrates induces a high improvement in the nanoparticles' catalytic performances [2,21,39]. This enhancement has been attributed to the strong interaction between nanoparticles and the support. Free nanoparticles in solution are used in electrocatalysis to find out the intrinsic activity of the electrocatalysts, especially the structure sensitivity [2]. While it is difficult to control, distinguish, and separate the intrinsic activity of the different crystallographic facets, the single crystal (bulk) as well as the shape-controlled nanoparticles constituted cornerstones for the fundamental understanding of electrocatalytic activity. Even if many examples can be found in the literature about the use of these kinds of electrocatalysts toward ORR and related reactions, they are not still yet proven as of any significant interest in FC sciences. Indeed, a support is needed to boost the current density when the catalyst is immobilized for the tests of the FCs. Their preparation and long-term storage processes are less competitive than supported nanoparticles. Besides, it is more difficult to produce these types of materials for large-scale applications such as for FCs.

### 2.2. Water-in-Oil (w/o) Microemulsion Method

The preparation of metal nanoparticles from the “water-in-oil” microemulsion (w/o) method was initiated by Boutonnet *et al.* [30] in 1982 when they reported the successful preparation of Pt, Pd, Rh and Ir nanoparticles with a size ranging from 3–5 nm. After this stage of initiation, it is worthy of note that the preparation of nanoparticles from this method was successful, particularly in the field of catalysis. It should be noted that the term “microemulsion” was introduced by the English chemist, J. H. Schuman [29,31,40,41]. According to Clause and co-workers, it can be assumed to be “a macroscopically monophasic fluid transparent compound made up by mixing water and hydrocarbon in the presence of suitable surface active agents (surfactants)” [42]. Similar definitions can be found in the literature [30,31,43]. It should be mentioned that this solution is optically isotropic and thermodynamically stable [44]. From a macroscopic point of view, the internal structure of the microemulsion appears to be homogeneous, but at the nanoscale, it is heterogeneous, consisting either of nano-spherical monosized droplets or a bi-continuous phase (10–40 nm) [41,44]. Obtaining this droplet is very crucial in order to control the size of the nanoparticles during their preparation.

The microscopic structure of the microemulsion is precisely determined at a given temperature by the ratio of its different constituents, as illustrated in Figure 2. Two systems can be clearly identified in this figure: the water-rich phase and the oil-rich one, determined by the water and oil contents. The

water-rich phase is obtained for a high concentration of water where the internal structure of the microemulsion consists of small oil droplets in a continuous water phase (micelles or direct micelles) and is known as “oil-in-water, o/w” microemulsion (ratio o/w  $\ll$  1). Indeed, to stabilize the system, the hydrophilic portion of the surfactant molecules must be oriented toward the aqueous phase (water), while the hydrophobic tail is directed toward the organic phase (oil) to form oil droplets. In nanoparticles’ preparation from colloidal methods, it is important to keep in mind that the droplet size is the key parameter for size, shape and control of other factors. Consequently, the system o/w is unusable for nanoparticles preparation because the metal ion (always in the aqueous phase) will be outside the droplet. Indeed, most metal precursors are inorganic salts and are soluble in water, not in oil [32]. At a high oil concentration, the system consists of small water droplets in a continuous oil phase (reversed micelles), also known as a “water-in-oil, w/o” microemulsion (ratio w/o  $\ll$  1). For the solution stabilization, the hydrophilic portion of the surfactant molecules oriented toward the aqueous phase (water) and the hydrophobic tail directed toward the organic phase (oil) form together a water droplet: reversed micelles which are water-in-oil droplets stabilized by a surfactant are obtained. Therefore, the system w/o (emulsions with low water concentration and high oil concentration) is used almost exclusively for nanoparticles’ preparation because the metal ion will be inside the droplet. It is a necessary condition for nanoparticles’ preparation from metal precursors. Furthermore, between these extreme situations, there is a bicontinuous phase without any clearly defined shape.

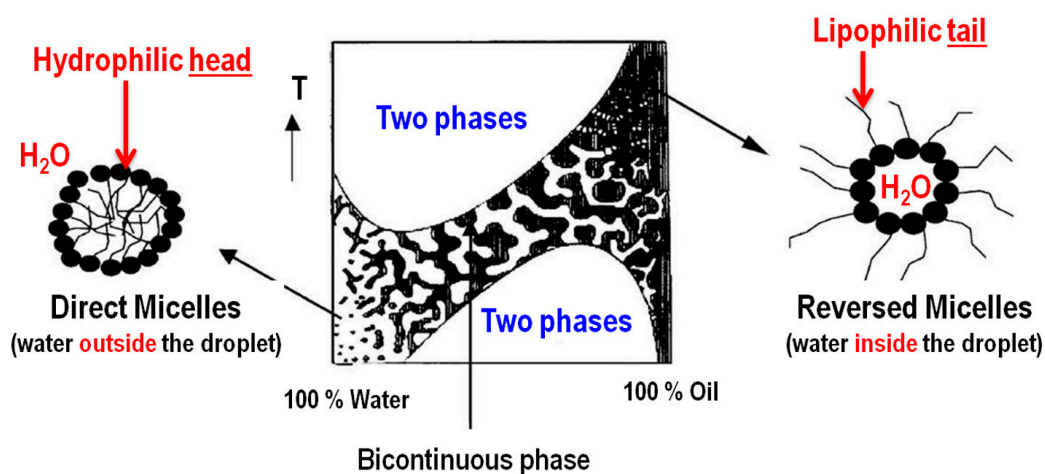


**Figure 2.** Scheme of the microscopic structure of a microemulsion at a given concentration of surfactant as function of temperature and water concentration, showing the different systems. Reprinted, adapted with permission from Ref. [44]: Copyright 2004, Elsevier and from Ref. [31]: Copyright 1995, American Chemical Society.

Obviously, at fixed water content, the volume of the surfactant plays crucial role for the size of the formed micelles. Basically, their size is inversely proportional to the amount of surfactant present in the microemulsion [32,44–46]. The surfactant can be ionic or non-ionic; its presence is very important for the stability of the microemulsion [31,44,45]. Moreover, the structure of micelles must be flexible to allow the penetration of the reducing agent and the interactions/exchanges between micelles during the collision step. In addition, when the ionic surfactants are used, they can form strong bonds with the surface of the nanoparticles. Thereby, it becomes particularly difficult to remove them during the cleaning step. This is

the case of sodium bis(2-ethylhexyl)sulphosuccinate, AOT, which can form thiol bonds with the metal surface, making it more complicated to remove. In order to minimize this kind of phenomenon, the most used non-ionic surfactant is a polyethylene glycol dodecylether known as Brij<sup>®</sup> 30 [47–50].

Concerning the nanoparticles' preparation, there are currently two main ways: either by preparing a second microemulsion (having the same composition as that containing the metal ions), which contains a reducing agent, or by direct addition of the reducing agent to the microemulsion that already contains metal salt precursors [44,51]. Figure 3 illustrates the formation of nanoparticles following the first procedure. Here, two microemulsions are mixed together, one containing the precursor and the other, the reducing agent. Due to the physical and chemical properties of its different constituents, the colloidal solution is very sensitive to temperature and the synthesis is currently performed at room temperature (20–25 °C) [34,49,50,52–56]. Current reducing agents are sodium borohydride (NaBH<sub>4</sub>), hydrazine (N<sub>2</sub>H<sub>4</sub>), gas hydrogen (H<sub>2</sub>) *etc.* The organic solvent (oil) can be hexane, n-heptane, cyclohexane or isooctane [44,47,55,56]. The formation of particles occurs in two steps known as the *nucleation process* inside the droplet and the *aggregation process* to form the final particle [44]. The major role of the surfactant is to control the growth via steric effect in order to have well-dispersed and homogeneous particles with a good size distribution.

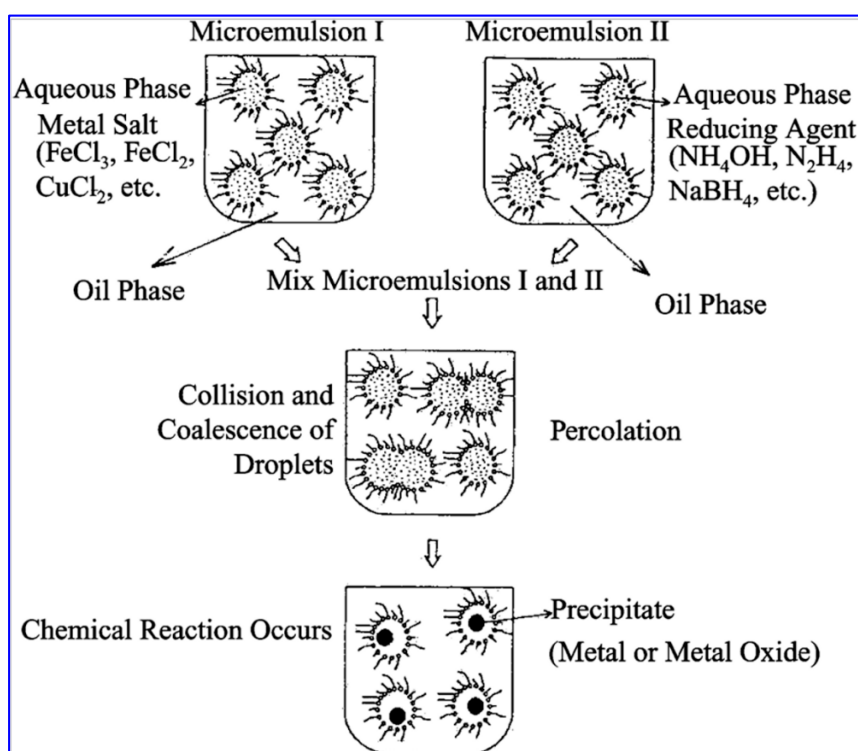


**Figure 3.** Proposed mechanism for the formation of metal particles from the microemulsion method using the two microemulsions protocol. Reprinted with permission from Ref. [45]. Copyright 2004, Elsevier.

Summarizing, the optimization of this method over more than twenty years has led to the following experimental parameters:

- molar ratio  $n_{(\text{water})}/n_{(\text{surfactant})}$ ,  $\omega$ : 3.8 [47,48,52,56],
- volume of organic solvent (*n*-heptane) per synthesis reactor: 27.35 mL [50],

- total metal salt concentration in the aqueous solution: 0.1–0.2 mol L<sup>-1</sup> [47,48,50],
- volume percentage of Brij<sup>®</sup> 30 in the microemulsion: 16.5% [47,48,52,56],
- molar ratio between the reducing agent and the metal salt: 15 [49,50,52,56],
- synthesis conducted at room temperature [34,49,50,52–56].

In order to have a good dispersion of nanoparticles, conducting and high surface area (BET surface) carbon substrates are currently used. The main roles of the support are to improve nanoparticles dissemination, to reduce the metal content (generally noble metals are used) and to provide good nanoparticles-support interactions [53,54,57]. Vulcan XC 72 and Vulcan XC 72R carbons are the most used substrates for electrocatalytic applications and the metal content rises from 20–40 wt.%. For this purpose, Vulcan carbon is thermally pre-treated (see Section 2.4) to remove the potential undesired contaminants coming from its industrial manufacture such as sulfur [53,54,57,58]. Very recently, it has been shown that this thermal activation highly improved the physicochemical and electrocatalytic properties of Vulcan [57]. We will briefly describe herein a typical synthesis as currently carried out in our research group, from two microemulsions: one containing the dissolved metal(s) precursor(s) and the other one, the reducing agent, NaBH<sub>4</sub>. Typically, microemulsions I and II (as shown in Figure 3) are mixed in a synthesis reactor thermostatted at 25 °C for about 30 min under magnetic stirring: the mixture gradually darkens, reflecting the formation of metal nanoparticles. Then, an appropriate amount of the Vulcan XC 72 or Vulcan XC 72R carbon is added after the solution has been transferred into an ultrasonic bath for homogenization (15–20 min), followed by additional vigorous stirring for 2 h. Finally the carbon supported metal nanoparticles are thoroughly filtered and washed to remove organic solvent and surfactant using three different solvents, acetone, ethanol and water. The filtration occurs under a vacuum system (Buchner) using a Millipore filter type GV 0.22 µm (also known as GVWP 0.22 µm). The washing steps are carried out strictly in the following order: addition of acetone, then ethanol and finally a mixture of 50 vol% acetone-water. It is strongly recommended to repeat this procedure at least three times. The material is rinsed thoroughly with Milli-Q<sup>®</sup> Millipore water (18.2 MΩ cm at 20 °C), and finally the filter containing the catalyst is removed and dried in an oven for at least 12 h at 75 °C. Figure 4 shows the low and high resolution TEM images of the bimetallic 40 wt% AuPt/C. From these physicochemical and electrochemical characterizations, Habrioux and co-workers found that the obtained bimetallic nanomaterials exhibit two different behaviors. For high Au-content, the Au-Pt particles exhibited alloy properties, and at low Au-content, atom rearrangement leads to an enrichment of the electrode surface with those of Pt. It should be mentioned that the AuPd/C bimetallic nanomaterials synthesized from w/o by Simões *et al.* [34] are unalloyed for Au ≥ 50 at%, leading to two phases: Au islets + AuPd alloy. Various studies have shown that ORR is a structure-sensitive reaction. This means that the crystallographic orientations (hkl) play a major role, more especially the low-index ones [2,4]. The seminal papers on the single crystal revealed that (111) and (110) are the most active facets toward ORR in aqueous media. Particularly, for Pt(hkl), the activity toward ORR increases in the order (100) < (110) ≈ (111) in HClO<sub>4</sub>; (100) < (110) < (111) in KOH and (111) ≪ (100) < (110) in H<sub>2</sub>SO<sub>4</sub> [2]. As highlighted in Figure 4b, the presence of (111) face on the nanoparticles prepared from the w/o approach allows better ORR efficiency to be expected on these catalysts.

Notwithstanding the diversity of applications, this method remains questionable due to the surfactant Brij<sup>®</sup> 30 that is not completely removed from the surface of the metal nanoparticles [59,60]. The

remaining molecules undoubtedly block some catalytic sites, therefore affecting the catalytic performances of the obtained catalysts. In conclusion, the nature of the surfactant (Brij<sup>®</sup> 30 or others) and its strong adsorption onto the metal nanoparticles' surface constitute the main drawback of the water-in-oil microemulsion method.

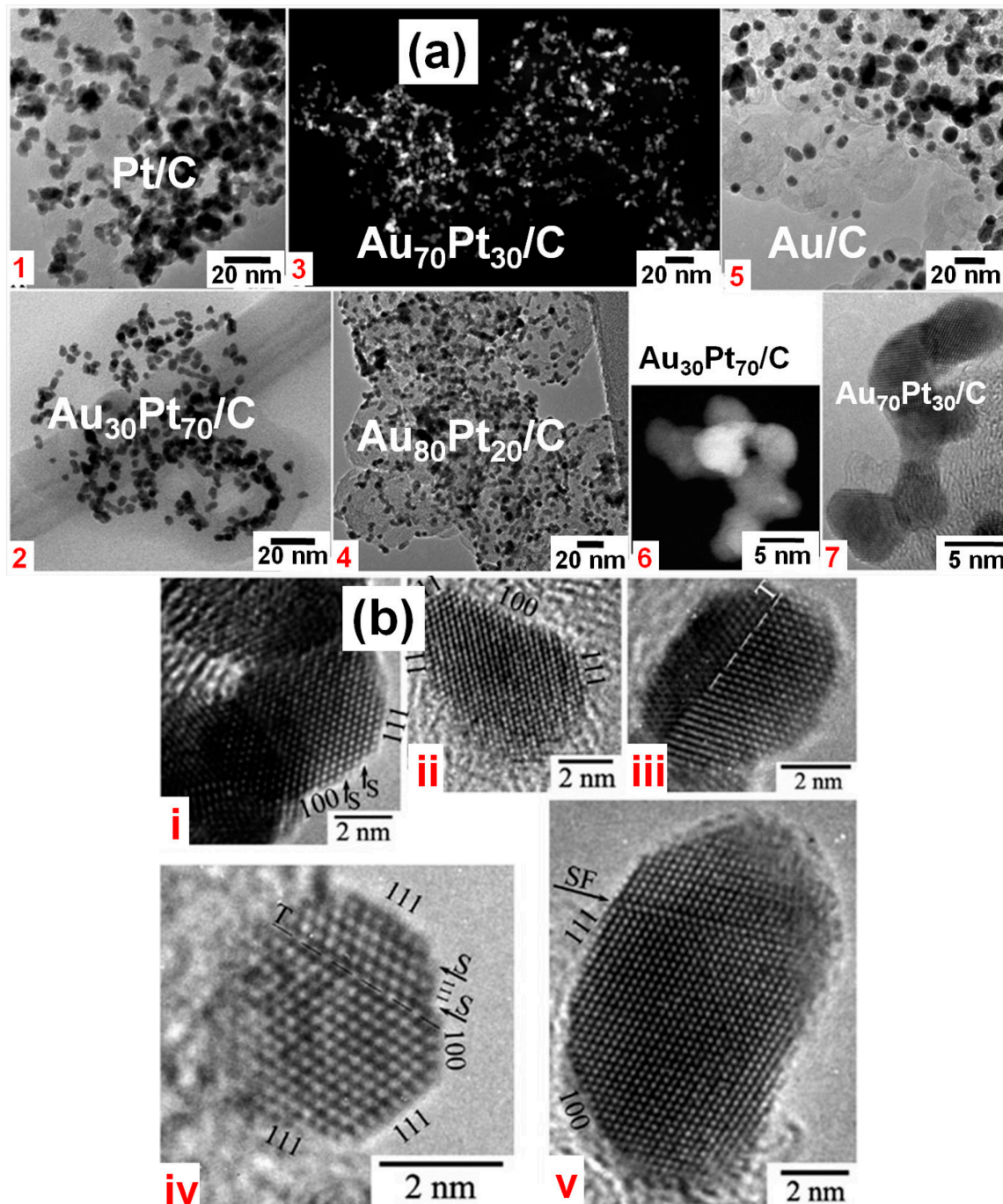
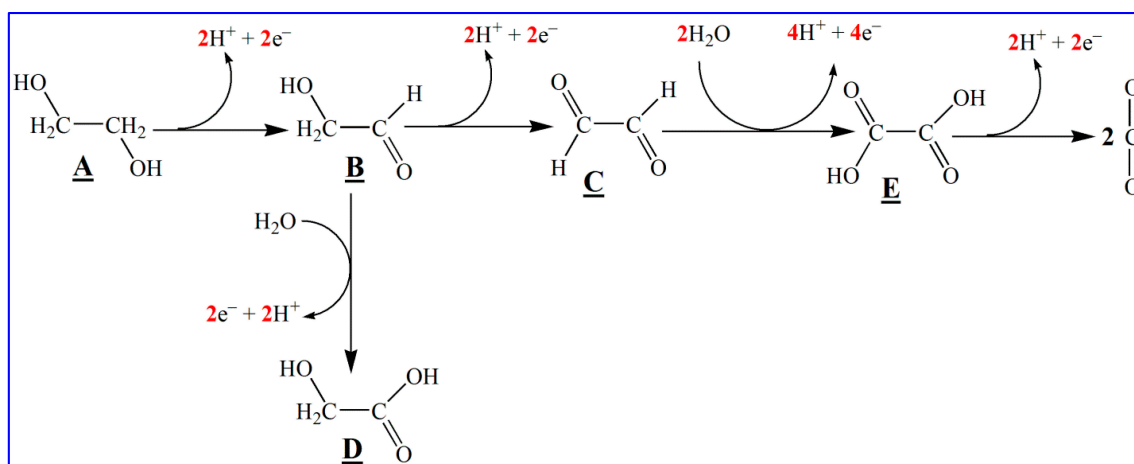


**Figure 4.** (a) TEM images of: (1) Pt/C, (2) Au<sub>30</sub>Pt<sub>70</sub>/C, (3) Au<sub>70</sub>Pt<sub>30</sub>/C, (4) Au<sub>80</sub>Pt<sub>20</sub>/C, (5) Au. Particle agglomerates are shown in (6) and (7) for Au<sub>30</sub>Pt<sub>70</sub>/C and Au<sub>70</sub>Pt<sub>30</sub>/C, respectively. (b) HRTEM images of (i and ii) Pt, (iii) Au<sub>30</sub>Pt<sub>70</sub>/C, (iv) Au<sub>70</sub>Pt<sub>30</sub>/C and (v) Au/C highlighting the facets, steps (S), twins (T) and stacking faults (SF). Note that the metal loading was 40 wt%. Reproduced and adapted in part from Ref. [54] with permission of the PCCP Owner Societies. Copyright 2009, Royal Society of Chemistry.





**Scheme 2.** Ethylene glycol (A) oxidation pathways to aldehydes (B, C), glycolic acid (D), oxalic acid (E) and further  $\text{CO}_2$  and carbonate in alkaline medium owing to interaction of  $-\text{OH}$  groups of ethylene glycol with metal-ion sites.

The oxidation of the ethylene glycol gives glycolate or glycolic acid (depending on the pH) which acts as a stabilizer for the metal species; the size of the noble metal colloids is thereby controlled through the pH value of the synthesis solution. Oxidation products resulting from the ethylene glycol oxidation reaction interact with the noble metal colloids and hence act as their stabilizers. Additionally, Skrabalak *et al.* [64] reported how metal ions are reduced by the ethylene glycol oxidation to glycolaldehyde, using a spectrophotometric method. They proposed an alternative pathway related to the reduction of metal precursor depending on the reaction atmosphere. For example, heating ethylene glycol between 140 and 160 °C in air, Equation (1), may generate glycolaldehyde as a reductant for the many metal precursors



It was found out from spectroscopic data that glycolaldehyde is the main reductant depending on reaction temperature, atmosphere, and experimental setup [64]. Numerous studies have been reported on synthesizing metal nanoparticles with controlled-size, shape and morphology, and satisfactory stability, as well as high product yield and low environmental contamination [65–67]. Physical properties of nanoparticles can influence catalytic activity [68,69], selectivity [70,71] and durability [72]. Biacchi *et al.* [73] demonstrated that proper selection of the polyol solvent can be used to manipulate the metal nanoparticles morphology. They reported that the kinetics and thermodynamics of nanoparticles synthesis is critically important for controlling the shape and size when using different polyol solvents such as ethylene glycol, diethylene glycol, triethylene glycol, and tetraethylene glycol. In recent years, methodological development of the synthesis of the highly active electrocatalysts has been one of the major topics in energy converting systems [74–79]. Joseyphus and co-workers [80] investigated the reaction rate of the polyol method using cobalt and its alloys. The reduction limit of polyol solution depends mainly on the concentration of hydroxyl ions ( $\text{OH}^-$ ) for the reduction of metal ions. Although the presence of  $\text{OH}^-$  ions in the metal ion-polyol system acts as a catalyst in accelerating the formation of precursor complexes, it may decrease the reaction rate by forming metal hydroxide compounds which are not easily reduced. Therefore, it is important to control the degree of complex or hydroxide forms in

the presence of  $\text{OH}^-$  ions by using UV-Visible spectroscopy. Susut and Tong demonstrated that the particle shape could be controlled in the presence of  $\text{AgNO}_3$  with different concentrations in the reaction mixture before the addition of PVP (poly-vinylpyrrolidone) and Pt precursor solutions [81]. Gonzalez-Quinjano *et al.* [82] also reported the synthesis of Pt-Sn/C electrocatalysts by using ethylene glycol containing ethanol and water in different ratios. They noticed that the chemical composition, lattice parameter, and degree of alloying depended on the solution ratio between ethylene glycol, ethanol, and water. The average particle size was observed as between 1.8 and 4.7 nm, the smaller particle sizes were reported in the absence of water. Furthermore, Jiang *et al.* [83] prepared Pt/C and Pt-Sn/C catalysts by slightly modifying the polyol method. In brief, they prepared a tin complex in ethylene glycol at 190 °C for 30 min and then added the required chloroplatinic acid and finally, the mixture was maintained at 130 °C for 2 h under argon gas to remove the oxygen and organic by-products. Lee *et al.* [84] prepared in ethylene glycol, acid pre-treated carbon supported Pt and Pt-Ni electrocatalysts, which exhibited significantly improved electrocatalytic activity.

In the polyol process, polyalcohols are currently used as both solvent and reducing agent. Alternatively, poly-vinylpyrrolidone (PVP) can be added as surfactant or capping agent [85,86] in association with a variety of reducing agents such as sodium borohydride ( $\text{NaBH}_4$ ) [87,88], and formaldehyde ( $\text{H-CHO}$ ) [88] for controlling surface reactivity. These properties significantly influence the electrochemical performance. During their synthesis, metal particles tend to aggregate, particularly in the liquid phase, because of their very high surface energy in the nano level. Therefore, nanoparticles have a natural tendency to be attracted to each other through Van der Waals forces leading to agglomeration. In order to neutralize the Van der Waals interaction, the required repulsive forces have to be improved. As a result, a stabilization procedure is required to ensure the quality of the nanomaterial products. The stability relation of the nanoparticles can be mainly controlled by two kinds of effects in the dispersing medium. One is an electrostatic stabilization (Figure 5a) for developing surface charges to repulse (high positive  $E_T$ ) aggregated particles, which can be evaluated by zeta potential measurements and the other is a steric stabilization (Figure 5b) for controlling the protective layer, using organic ligands and polymer [89].

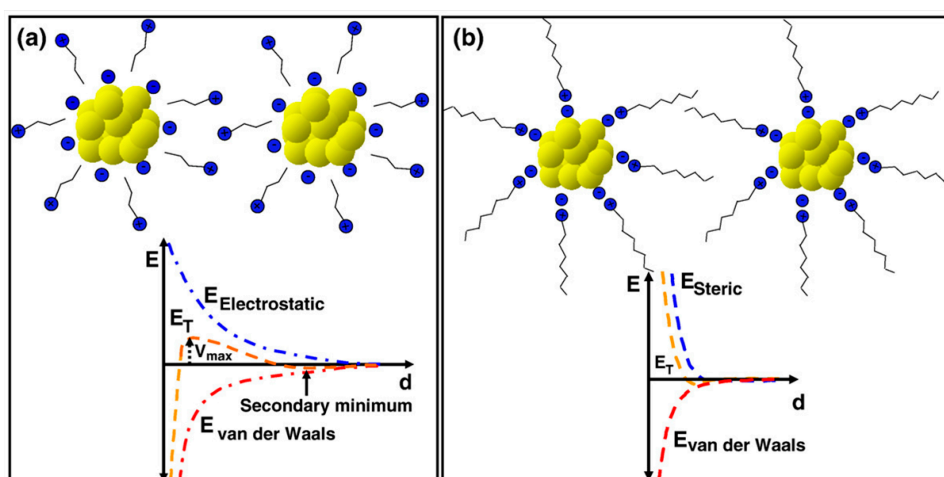


**Figure 5.** Stabilization of nanoparticles in a dispersing medium; (a) electrostatic stabilization and (b) steric stabilization of metal. Reprinted with permission from Ref. [89]. Copyright 2004, Elsevier.

#### 2.4. Impregnation-Reduction Process

The impregnation-reduction method is one of the simple and straightforward techniques in material science for supported nanocatalysts preparation. It is still widely used in the field of gas-phase heterogeneous catalysis to prepare nanostructured catalysts. Compared to the w/o method, the impregnation technique is one of the green class methods to prepare nanocatalysts due to its environmental friendly solvents *versus* organics ones. The synthesis takes place either at low or room temperatures, thus minimizing energy consumption [32,51]. For a long time, this chemical approach was devoted to Pt-Ru catalyst preparation [90–92]. Basically, it involves two steps: impregnation and reduction. During the impregnation, the support (mainly carbon) is immersed in the aqueous solution containing the desired metal precursors. Then, metal ions are reduced to their metallic state by the addition of an aqueous solution of reducing agent such as  $\text{Na}_2\text{S}_2\text{O}_3$ ,  $\text{NaBH}_4$ ,  $\text{Na}_4\text{S}_2\text{O}_5$ ,  $\text{N}_2\text{H}_4$ , H-CHO, or  $\text{H}_2$  [51,91,93,94]. It should be noted that the impregnation duration step strongly depends on the nature of the precursors, the targeted metal loading, as well as the nature of the support. Recently, Knani *et al.* [93,95] optimized an experimental approach for synthesizing methanol tolerant ORR nanocatalysts (10 wt% Pt-Co-Sn/C) preparation using  $\text{NaBH}_4$  and Vulcan XC 72R carbon as reducing agent and support, respectively. Typically, the mixture made of metal precursors and the support is ultrasonically homogenized for 30 min followed by additional stirring for 2 h before the reduction step at 80 °C. Then, the filtered solid composite is washed several times with ultra pure water and dried in an oven at 110 °C for about 4 h [95]. Miller *et al.* [96], reported the preparation of noble metal free electrocatalysts based on iron(II) and silver(I) phthalocyanines using an impregnation-reduction method. During this procedure the Ketjenblack EC-600JD used as support was impregnated with the metal precursors by stirring (30 min) and sonicating (30 min) ethanol suspensions (200 mL) of the metal phthalocyanine complexes with the carbon material at room temperature. The obtained mixture was stirred afterwards for 24 h (to improve the impregnation process with the support surface) at room temperature and then sonicated for 30 min again. After these steps, the solvent was removed under reduced pressure to yield a solid residue which was dried under high vacuum. Then, the resulting powder annealed at high temperature (250–800 °C) for 2 h was cooled to room temperature under continued argon flow prior to use. These nanostructures have shown good electrochemical performances toward ORR in alkaline medium. Others impregnation-reduction processes have been reported for the successful preparation of PtRhM/C (M = W, Pd, or Mo) [97]; PtRh/C [98]; PtNi/C [99].

Different metal precursors can be used; chloride, sulfite, nitrate, carbonyl complexes. It should be emphasized that the metal carbonyl complexes are especially interesting since the second step is not required in some cases [32,100]. As any process, many experimental parameters affect the electrochemical activity of the obtained catalysts by controlling their composition, morphology, and dispersion onto the support. From the experimental view, it has been suggested that, the control of the nanoparticles size and as yet the particle distribution are more difficult by the impregnation method, which thus constitutes its major drawback [32,51].

### 2.5. Bromide Anion Exchange (BAE) Method

Obviously, electrocatalysis is one of the disciplines that requires maximum cleanness. Indeed, from catalyst preparation to initiating chemical reactions, the cleanliness is mandatory throughout the chain. Any impurity can drastically alter the catalytic activity/selectivity through the control of active sites. Thus, taking into account the fact that the reactions involved in electrocatalysis are surface reactions, the electrocatalyst surface state (cleanness) is the key parameter for the best electroactivity. Thereby, the surface of the nanomaterial must be free from impurities such as surfactant molecules and other capping ones. In this way, the development of an advanced synthetic method must limit the use of strong organic molecules, which have an affinity with the nanoparticles surface. To this end, the research group of Prof. B. Kokoh has recently initiated a new clean, easy, and accessible synthetic route called “Bromide Anion Exchange, BAE” [36,38,101]. Most of the metal salts (precursors) used in nanomaterials synthesis are chlorinated. The bromide ion ( $r(\text{Br}^-) = 195 \text{ nm}$ ) is larger than its counterpart chloride ( $r(\text{Cl}^-) = 181 \text{ nm}$ ). Thus, the partial or total substitution of  $\text{Cl}^-$  by bromide anions must accentuate steric hindrance around the metal cation, which will further play a crucial role during the seed's growth. This advanced method has been successfully used to synthesize Au-based nanocatalysts for glucose electro-oxidation [38,57], Pd-based electrocatalysts for glycerol electro-oxidation [36,37,101] and hybrid/abiotic electrodes for biofuel cell application [102,103].

This convenient and straightforward synthesis approach is an environmentally friendly method and is based on the use of bromide ion as a capping agent, the major gate in the BAE process. It has been reported that halide ions (chloride, bromide, and iodide) could serve as coordination ligands and thus, play the role of capping agent for shape and size control of nanocrystals [67,104–107]. Figure 6 summarizes the different steps for preparing nanocatalysts with the BAE route. The main feature of BAE lies in the simplicity undertaken. By using no organic compounds as surfactants or capping agents, clean, small, and well-dispersed nanoparticles with highly improved catalytic properties are currently obtained. The effects of the different parameters such as the metal salt concentration, the amount of bromide anion and the temperature of the synthesis reactor were scrutinized recently. From these reports, the molar ratio between KBr and total metal(s):  $\phi = n(\text{KBr})/n(\text{metal(s)})$  is 1.46; the total molar concentration of metal salts is 1 mM and the reactor temperature is 25 and 40 °C (meaning 25 °C before the addition of the reducing agent and 40 °C after) [108].

Typically, the metal precursor salts are dissolved in a reactor containing ultrapure water thermostatted at 25 °C under magnetic stirring. Then, an appropriate amount of KBr via the parameter  $\phi$  is added under vigorous stirring. A suitable amount of carbon support (Vulcan or Ketjenblack) is then added under constant ultrasonic homogenization for 45 min, followed by the drop wise addition of the reducing agent, under vigorous stirring. Afterwards, the reactor temperature is elevated tot 40 °C (to improve the reaction kinetics) for a 2 h period. Finally, the carbon supported nanomaterials are filtered, washed several times with ultra pure water and dried in an oven at 40 °C for 12 h. In the whole BAE procedure, the Vulcan or Ketjenblack supports were thermally pretreated at 400 °C under nitrogen atmosphere for 4 h, in order to improve their physical properties and remove any contaminant coming from their industrial manufacture [57]. Holade *et al.* [57] found surprisingly that the BET surface area of the support was enhanced, being 322 and 1631  $\text{m}^2 \text{g}^{-1}$  instead of 262 and 1102  $\text{m}^2 \text{g}^{-1}$  for the as-received Vulcan XC 72R (C) and Ketjenblack EC-600JD (KB) materials, respectively. They

also found that Pt/C and Pt/KB exhibited a highly improved specific electrochemical surface area (SECSA). It is worthy of note that all catalysts were prepared with a high chemical synthesis yield ( $\omega > 90\%$ ), defined as the percentage of the ratio between the experimental mass and the theoretical one based on the initial reactor mixture [102,103]. It should be emphasized that it is the first time that such a synthesis yield has been reported. Indeed, for electrocatalysts preparation, neither the microemulsion method [30,109] nor any of the others [14,35,110,111] yielded this important result, indicating that the BAE method is suitable for nanomaterials preparation.

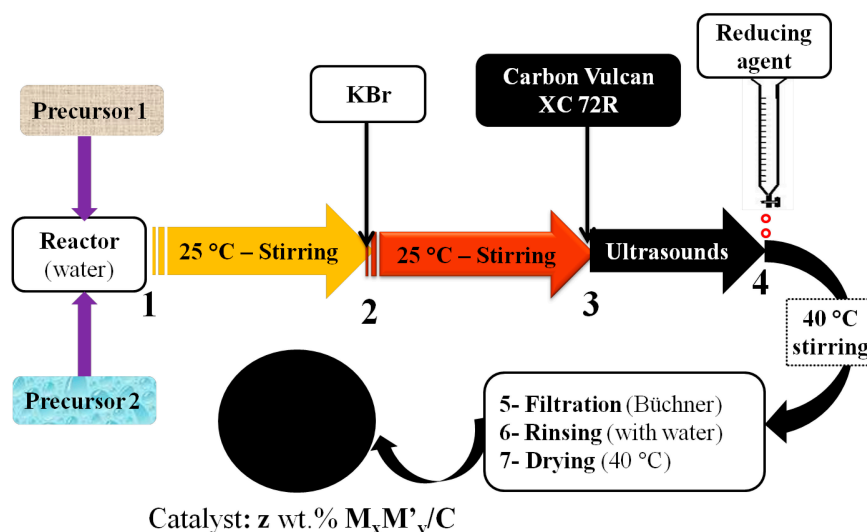


**Figure 6.** The experimental setup of the Bromide Anion Exchange (BAE) route for nanoscale materials synthesis. Reproduced with permission from Ref. [37] Copyright 2014, The Electrochemical Society.

During the synthesis (before the reduction step), change of the initial solution color was observed after the addition of KBr (see Figure 6: before and after step 2). Color changes can be seen in Figure 7a,c,e. To gain further insights on the origin of this phenomenon, UV-Vis measurements were performed. As can be seen in Figure 7b,d,f, there is a change in the UV-Vis spectra on the addition of KBr. In the case of the Pt salt, the addition of KBr shifts the band at 287 nm toward 298 nm with an intense shoulder around 411 nm. The absorption band due to a ligand-to-metal charge transfer transition of the  $[PtCl_6]^{2-}$  ion complex is found to be at 263 nm [112] or 260 nm [46,113,114]. Thus, the shift and intensity of the present bands indicate partial substitution of  $Cl^-$  in the  $[PtCl_6]^{2-}$  ion complex by  $Br^-$ . For the Pd salt, the aqueous solution goes from a clear yellow to a deep yellow, depending on the metal salt concentration. Furthermore, the addition of KBr to this solution drastically changes its appearance. According to the literature, the absorption wavenumber associated with the complex  $[PdCl_4]^{2-}$  in aqueous solution may be 425 nm [115] or 415 nm [116]. This value depends undoubtedly on the complex ion concentration in the solution and could be affected by the presence of other species. The metal salt solution without KBr presents a band at *ca.* 300 nm and a shoulder at *ca.* 400 nm. With KBr, in addition to the band at 325 nm, two shoulders at 400 nm and 510 nm can be observed. The slight shift of the peak position and the appearance of the band around 510 nm indicate clearly the insertion of the  $Br^-$  ions in the complex  $[PdCl_4]^{2-}$ . Herein, the ratio  $n(Br^-)/n(Pd^{2+})$  is 1.5 *versus* 4 for the complex ion  $[PdBr_4]^{2-}$ . Thus, there is no complete substitution of chloride by bromide.

The change of the color, substantiated with the UV-Vis observations is attributed to the complex ion  $[\text{PdCl}_{4-x}\text{Br}_x]^{2-}$ ,  $0 \leq x \leq 4$ . Klotz *et al.* [117] reported that, in aqueous media,  $[\text{PdI}_4]^{2-}$  is  $10^{8.1}$  times more stable than  $[\text{PdBr}_4]^{2-}$  which is  $10^{4.1}$  times more stable than  $[\text{PdCl}_4]^{2-}$ . Consequently, the complex ions that control the particles size/shape growth after reduction is  $[\text{PdCl}_{4-x}\text{Br}_x]^{2-}$ . The latter species provides a more steric environment than  $[\text{PdCl}_4]^{2-}$ . This hypothesis was confirmed when nanoparticles were synthesized without and with different amounts of KBr [108].

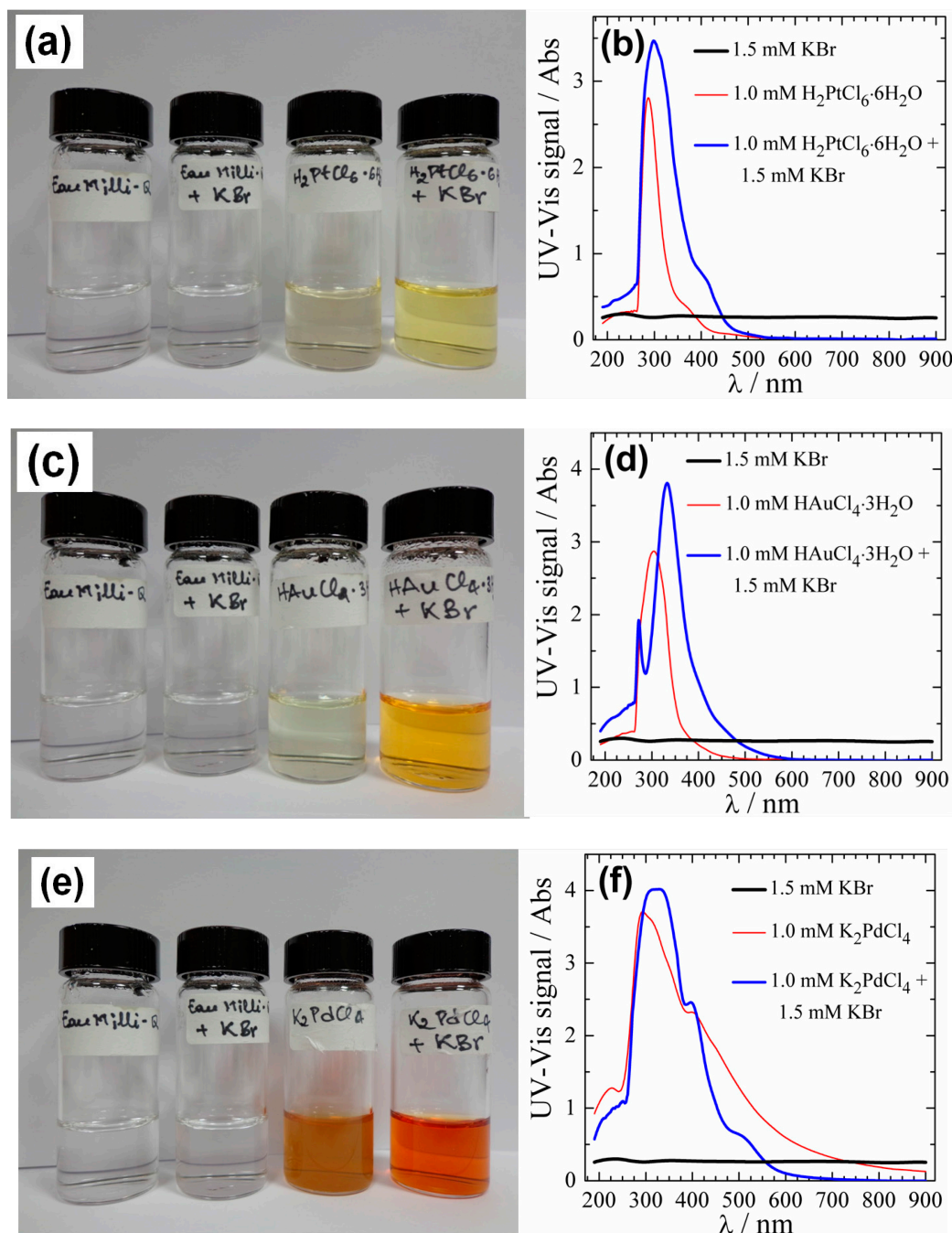


**Figure 7.** (a), (c) and (e) From left to right in each photograph, images of water containing: no substance, 1.5 mM KBr, 1.0 mM metal salt and 1.5 mM KBr + 1.0 mM metal salt. (b), (d) and (f) Their corresponding UV-Vis absorption spectra of water containing 1.5 mM KBr (black), 1.0 mM  $\text{H}_2\text{PtCl}_6 \cdot 6\text{H}_2\text{O}$  (red) and 1.5 mM KBr + 1.0 mM  $\text{H}_2\text{PtCl}_6 \cdot 6\text{H}_2\text{O}$  (blue). Note: (a–b) for platinum; (c–d) for gold and (e–f) for palladium.

Figure 8a,b show the TEM micrographs (with their HRTEM images in the inset) of 20 wt% AuPt nanomaterials and their corresponding particle size distribution when using Vulcan XC 72R or Ketjenblack EC-600JD as supports, respectively. Particles are well dispersed onto the support with a mean particle size between 3–6 nm. The HRTEM images highlight an octahedron-like shape. It has been observed that for Au-based bimetallics, the particle size increases with increasing Au content, which is a well-known phenomenon, coming from the difference in the reduction kinetics of the metal salts. Trimetallics AuPtPd supported on both Vulcan and Ketjenblack were also successfully prepared from BAE [102,103].

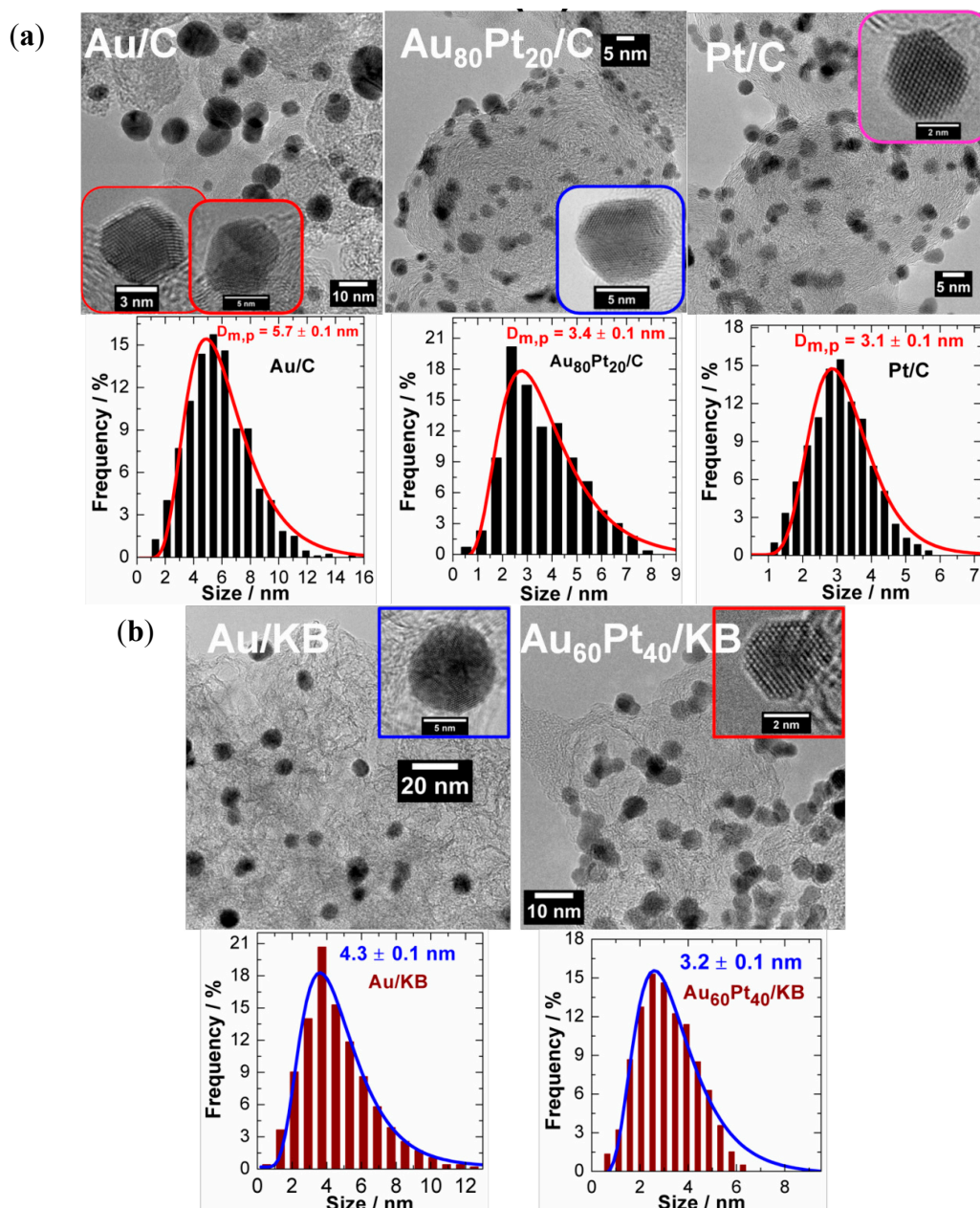


**Figure 8.** TEM-HRTEM micrographs and their corresponding particle size distribution (histograms were fitted using the log-normal function) of the nanostructured AuPt (20 wt%) supported on (a) Vulcan XC 72R and (b) Ketjenblack EC-600JD. (a) Reprinted and adapted with permission from Ref. [103]. Copyright 2014, John Wiley & Sons, Inc. (b) Reprinted and adapted with permission from Ref. [102]. Copyright 2014, John Wiley & Sons, Inc.

## 2.6. Other Synthetic Routes

From chemical to physical approaches, a huge number of metal nanoparticles preparation methods have been initiated over the last twenty years. Formerly reserved for the application in physics and related fields [26,39], nanomaterials prepared from physical routes are becoming unavoidable targets for electrocatalysis. Free nanoparticles prepared in solution from radiolysis [118] or laser ablation processes have been successfully tested in electrocatalysis [119]. Up till now, no test has been performed using carbon as support for application in electrocatalysis. The other chemical methods are the historical methods developed by Bönemann and co-workers [94,120,121]. They have been adapted for electrocatalysts preparation [58,94]. In such a method, the reducing agent is a tetra-alkylammonium triethylborohydride, which acts also as a surfactant after reducing the metal salt in a tetrahydrofuran medium. After addition of the support, e.g., Vulcan XC 72 carbon, the filtered powder is calcined under air at 300 °C. Small nanoparticles about 2–5 nm are currently obtained. However, because of the use of some organic molecules as reducing agents, their removal from the nanoparticles surface is not always effective. Thus, their catalytic performance can be affected.

## 3. Application of Carbon-Supported Nanocatalysts toward the ORR

### 3.1. ORR Activity on Various Carbon Supported Nanoparticles Prepared from w/o Method

Because of its natural abundance (20.95 vol%; 23.20 wt% of the earth's atmosphere and roughly 21% in air), dioxygen is the first choice of oxidant used at the cathode in FCs. Already known as an oxidant in the propulsion system, H<sub>2</sub>O<sub>2</sub> can supply O<sub>2</sub> as in the case of submarines. From this perspective, FCs were already developed [122,123]. This section will focus on the electrocatalytic performances of carbon-based substrates supporting metal nanoparticles toward the ORR. An emphasis on analyzing data from theoretical models to address the intrinsic and specific electrocatalytic properties depending on the synthetic method is incorporated throughout. The issue of the ORR is as old as that of FCs. Obviously; it is certainly one of the most widely studied processes due to its important applications in the field of clean energy conversion and storage systems. The ORR involves several basic steps. To date, two plausible mechanisms have been proposed in the literature (Figure 9) [124–126]. According to Acre *et al.* [125], the direct O<sub>2</sub> reduction to H<sub>2</sub>O (path A) is the result of O<sub>2</sub> adsorption parallel to the catalytic surface plane. This requires the presence of active sites side by side. The other pathway (path B) proceeds by an initial adsorption of O<sub>2</sub> perpendicularly to the electrode surface (by a single atom). However, it should be noted that the second step (reduction of H<sub>2</sub>O<sub>2</sub>) has a high activation energy, which increases the overpotential.

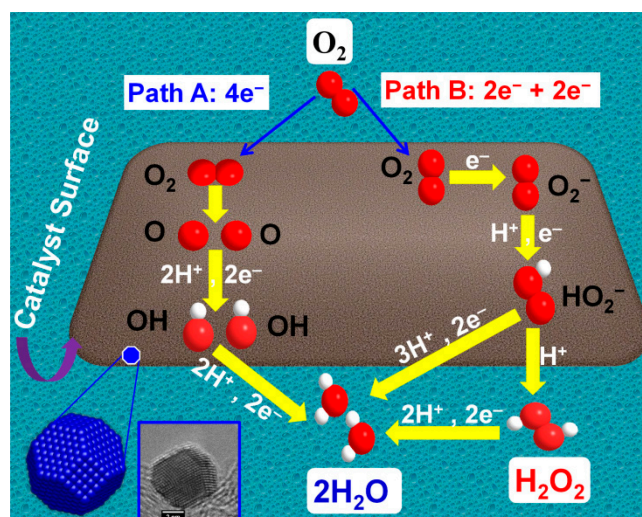


**Figure 9.** Schematic representation of the oxygen reduction reaction (ORR) mechanism by direct pathway (A: adsorption parallel to the surface) and indirect pathway (B: adsorption perpendicular to the surface). Reprinted and adapted with permission from Ref. [125]. Copyright 1997, Elsevier.

In the early 2000s, most of the catalytic applications of nanomaterials prepared from the water-in-oil method (developed more than 10 years ago) were oxidation of organic molecules in heterogeneous catalysis ranging from batch reactor to electrocatalysis. Tuning the experimental factors that affect the w/o method will be crucial for designing more active low temperature FCs cathodes. In 2008, Demarconay and co-workers reported the use of the w/o route to prepare various Pt-Bi bimetallic nanomaterials dispersed onto Vulcan XC 72 carbon (metal loading: 50 wt%) [33] for the oxygen reduction reaction in alkaline medium. It is worth mentioning that this metal loading is too high to achieve the condition for commercialization of FCs which is limited to 8 g of platinum group metals (PGM) per vehicle, meaning less than  $100 \mu\text{g}_{\text{PGM}} \text{cm}^{-2}$  at the cathode [9]. However, it can be helpful to understand the ORR electrocatalysis before thinking about the required three major criteria for FCs MEAs: cost, performance, and durability. In this preliminary ORR investigation using electrocatalyst from the w/o method, the RRDE technique to find out the fundamental data was used. It is worthy of note that, after the preparation of a carbon black catalyst, a black powder is obtained. Before using this powder for electrochemical tests, a catalytic ink is prepared. To this end, different approaches are currently used and are based on the initial method proposed at the beginning of the 1990s using Nafion<sup>®</sup> suspension [101,127–129]. Figure 10 shows the polarization curves at  $5 \text{ mV s}^{-1}$  (2500 rpm) at the disc for Pt/C, Vulcan XC 72R and different bimetallic catalysts in 0.2 M NaOH. The reaction starts at *ca.* 1.05 V *vs.* RHE on PtBi/C and 0.87 V *vs.* RHE on Vulcan XC 72R. An onset circuit potential (OCP) of 1.05 V *vs.* RHE reflects the ORR sluggishness because it must be roughly 1.19 V *vs.* RHE. As can be seen in the activation–diffusion mixed region (from 1.0–0.7 V *vs.* RHE) the bimetallics Pt<sub>90</sub>Bi<sub>10</sub>/C and Pt<sub>80</sub>Bi<sub>20</sub>/C are more active than Pt/C and Pt<sub>70</sub>Bi<sub>30</sub>/C. This means that the optimum window is obtained when at %Bi < 70 in the PtBi alloy system. The Pt/C catalyst synthesized by this method did not produce any peroxide, yielding roughly 4 as the number of exchanged moles of electron per mole of oxygen as on bulk Pt [130]. The evaluated kinetic current density at 0.95 V *vs.* RHE was 0.60, 1.05, 1.14, and 0.49  $\text{mA cm}^{-2}$  on Pt/C, Pt<sub>90</sub>Bi<sub>10</sub>/C, Pt<sub>80</sub>Bi<sub>20</sub>/C, and Pt<sub>70</sub>Bi<sub>30</sub>/C,

respectively. Unfortunately, it was not always mentioned whether this kinetic current density, which is free from mass transport, was evaluated using geometrical or active surface area. Therefore, it is difficult to compare it with other values found in the literature. Based on these values, Pt<sub>80</sub>Bi<sub>20</sub>/C shows the best kinetic activity. The value of exchange current density ( $j_0$ ) at the high overpotential region on this electrode material is  $23.2 \cdot 10^{-3} \text{ mA cm}^{-2}$ , which is higher than 16.8 and  $5.6 \cdot 10^{-3} \text{ mA cm}^{-2}$  on Pt/C and Pt<sub>70</sub>Bi<sub>30</sub>/C, respectively. Typically the exchange current density is  $5.4 \cdot 10^{-5} \text{ mA cm}^{-2}$  on the bulk Pt [130]. The low value of the Tafel slope on Pt<sub>70</sub>Bi<sub>30</sub>/C at high overpotential ( $99 \text{ mV dec}^{-1}$ ) contrary to theoretical value of  $120 \text{ mV dec}^{-1}$  has been explained by the presence of bismuth oxides. Table 1 shows the influence of the synthesis method and catalyst composition on the kinetic parameters. More importantly, the authors found that Pt<sub>80</sub>Bi<sub>20</sub>/C exhibits a high tolerance for ORR in the presence of 0.1 M ethylene glycol from 1.0–0.9 V vs. RHE. Indeed, they investigated the tolerance properties of the catalysts towards the ORR in the presence of ethylene glycol as fuel. The platinum substitution by bismuth up to 20 at% improves the catalyst tolerance by shifting the reduction wave towards higher potentials. These kinds of fuel tolerant cathode materials are promising electrodes for the development of advanced electrocatalysts for direct alcohol fuel cells in which the fuel can crossover the membrane to be mixed with O<sub>2</sub> in the cathodic compartment.

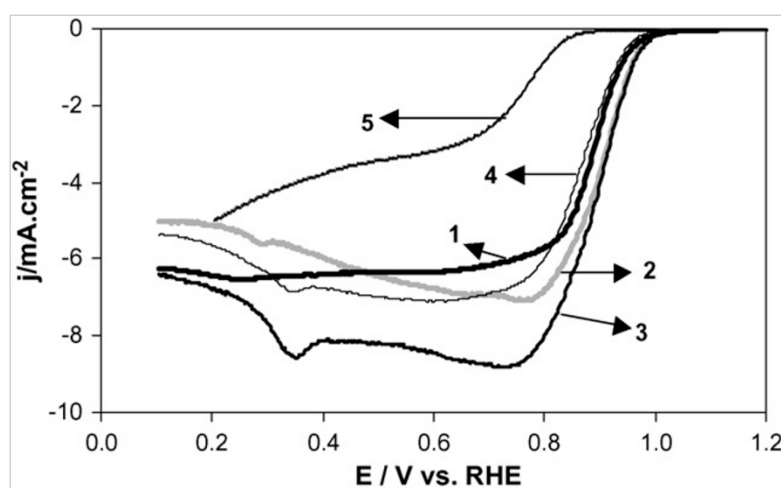


**Figure 10.** ORR polarization curves recorded in an O<sub>2</sub>-saturated 0.2 M NaOH solution at 50 wt.% PtBi/C catalysts prepared from w/o method: (1) Pt/C, (2) Pt<sub>90</sub>Bi<sub>10</sub>/C, (3) Pt<sub>80</sub>Bi<sub>20</sub>/C, (4) Pt<sub>70</sub>Bi<sub>30</sub>/C and (5) Vulcan XC 72 carbon ( $5 \text{ mV s}^{-1}$ , 2500 rpm, 20 °C). Metal loading on the electrode:  $177 \mu\text{g cm}^{-2}$ . Reprinted with permission from Ref. [33]. Copyright 2004, Elsevier.

Until the early 2000s, it was difficult to decrease the metal content in the electrocatalysts without losing significant catalytic activity. This poses a considerable challenge to the material science community, particularly when considering that for most catalyst systems, durability and high current density work together with the PGM content. Habrioux and co-workers used the same w/o method to design platinum-gold nanoalloys with improved electrocatalytic properties [52]. They managed to reduce the metal charge up to 40 wt% without a significant loss in catalytic activities. Au is known to improve the Pt electrode durability by modifying the Pt–OH bond strength [52]. O<sub>2</sub> reduction starts at *ca.* 0.7 V vs. RHE on Vulcan, 0.9 V vs. RHE on Au/C and 0.95 V vs. RHE on Au<sub>70</sub>Pt<sub>30</sub>/C, Au<sub>20</sub>Pt<sub>80</sub>/C, and Pt/C. The peroxide production increases when the Pt content decreases in the electrode materials.

From the kinetic parameter, Au<sub>70</sub>Pt<sub>30</sub>/C has the best exchange current density:  $j_0 = 300, 300, 700, 100$  and  $400 \mu\text{A cm}^{-2}$  for Pt/C, Au<sub>20</sub>Pt<sub>80</sub>/C, Au<sub>70</sub>Pt<sub>30</sub>/C Au/C, and Vulcan carbon, respectively. In order to reduce the cost of the electrocatalysts, while keeping the same reaction kinetics, Pd-based electrodes have been recognized to be excellent candidates. Precisely, the addition of Ni or Ag boots the electroactivity of Pd either for oxidation of organic molecules [36,101,108] or ORR [56,131] in both acid and alkaline media. The synthesis of 2–5 nm of PdAg/C and PdNi/C (20 wt%) from the w/o method using the reversed micelles approach has been reported [56]. The polarization curves for ORR on Pd/C, Pd<sub>70</sub>Ni<sub>30</sub>/C, and Pd<sub>70</sub>Ag<sub>30</sub>/C electrode materials are represented in Figure 11. In the activation region (0.95–0.85 V vs. RHE), the addition of the second metal to Pd does not induce any benefit in terms of activity. The electrodes' efficiency in terms of oxygen reduction current follows the order Pd/C > Pd<sub>70</sub>Ni<sub>30</sub>/C > Pd<sub>70</sub>Ag<sub>30</sub>/C. This is supported by the value of the exchange current density ( $j_0$ ), which is 11.1, 7.4 and  $1.6 \mu\text{A cm}^{-2}$  for Pd/C, Pd<sub>70</sub>Ni<sub>30</sub>/C, and Pd<sub>70</sub>Ag<sub>30</sub>/C, respectively [56]. In the mixed activation-diffusion limiting control domain (0.85–0.65 V vs. RHE, Figure 11), the presence of Ag or Ni increases slightly the limiting current, which is roughly  $6.9 \text{ mA cm}^{-2}$  (Pd/C),  $7.1 \text{ mA cm}^{-2}$  (Pd<sub>70</sub>Ag<sub>30</sub>/C), and  $8.0 \text{ mA cm}^{-2}$  (Pd<sub>70</sub>Ni<sub>30</sub>/C). The determined number of exchanged electrons, from Koutecky-Levich plots, is close to 4 for all the catalysts. This shows that O<sub>2</sub> reduction is a four-electron transfer process for the electrode potential centered at *ca.* 0.85 V vs. RHE. But, the careful analysis of the two behaviors in the polarization curves (on the disc) in 0.9–0.8 V vs. RHE and 0.75–0.6 V vs. RHE indicates a 2 + 2 electrons process.

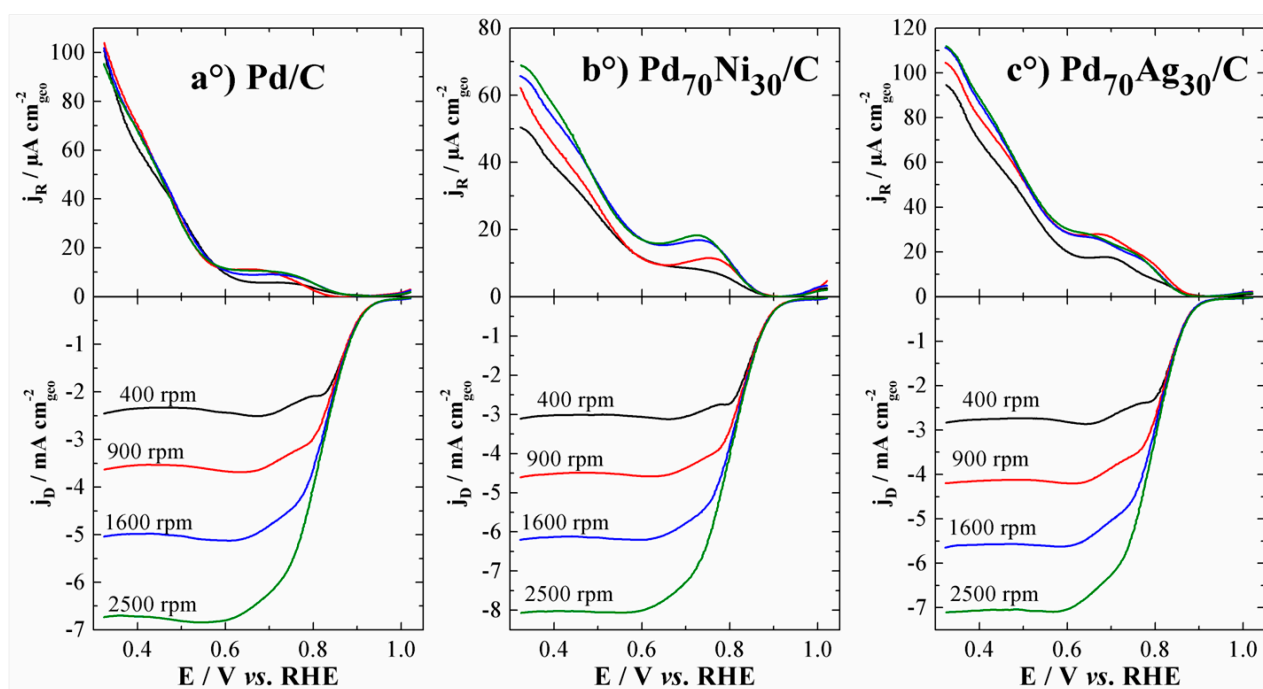


**Figure 11.** Disc (bottom) and ring (top) current-potential curves for ORR on (a) Pd/C, (b) Pd<sub>70</sub>Ni<sub>30</sub>/C and (c) Pd<sub>70</sub>Ag<sub>30</sub>/C electrocatalysts prepared from w/o method (20 wt%), in O<sub>2</sub>-saturated 1 M NaOH at  $5 \text{ mV s}^{-1}$ . Metal loading on the electrode *ca.*  $100 \mu\text{g cm}^{-2}$ .

### 3.2. ORR Activity on Various Carbon Supported Nanoparticles Prepared from the Polyol Method

Examination of the oxygen reduction reaction on various metals, including Pt, Pd, Rh, Ir, and Au began in the 1960s. Over the past decade the polyol process has been used to synthesize metallic nanoparticles such as Pt [132,133], Pd [88,134], Au [135], Fe [136], Ni [137,138], Co [139], Ag [140,141], Cu [142,143], Sn [144], and Rh [73]. Platinum is one of the most active metal catalysts toward many electrochemical reactions, such as oxidation of small molecules and reduction of molecular oxygen in PEMFC. Compared to other transition metals, Pt adsorbs oxygen with an intermediate bond strength. That is, Pt adsorbs oxygen strongly enough to be reduced, but not so strongly that the surface oxidizes. Additionally, the transition metals, for instance Ni, Co, Cr and Fe, adsorb oxygen so strongly that the surface may fully oxidize, while Au adsorbs oxygen so weakly that it does not stick to the surface. As platinum exhibits the highest catalytic activity for the oxygen reduction reaction [145], carbon supported platinum-based bimetallic alloys have been investigated as electrocatalysts to reduce the voltage losses associated with the cathode performance. Platinum-based bimetallic catalysts provide high oxygen reduction activity on the basis of d-band modification by the addition of a second metal. Toda *et al.* [146] reported that oxygen adsorption increases in the case of changing of the electronic structure of Pt induced by a transition metal, and then the O-O bond is weakened. For this purpose, various platinum-based bimetallic catalysts, such as Pt-Ni [147,148], Pt-Co [149,150], Pt-Fe [151,152], Pt-Cr [153,154], Pt-Cu [155,156], Pt-V [157,158], Pt-Mn [159], Pt-Bi [35], Pt-Te [160] have been reported. It can be clearly emphasized that modified-platinum catalysts display 1.5–3 times higher catalytic activity than that of pure platinum catalyst. Alvarez *et al.* [88] reported oxygen reduction activity on carbon supported palladium prepared by using ethylene glycol, sodium borohydride, and formaldehyde. They showed that reduction of the palladium precursor salt in alkaline medium led to small palladium nanoparticles around 5.7 nm at pH 11. It is clearly displayed that the peak position for palladium oxide reduction depends on the nanoparticles size. Indeed, this peak is centered at 0.70 V vs. RHE on Pd/C-E-TEK; 0.72 V vs. RHE on Pd/C-CH<sub>2</sub>O, 0.74 V vs. RHE on Pd/C-NaBH<sub>4</sub> and 0.74 V vs. RHE on Pd/C-EG. Rao *et al.* [152] reported Pt and Pt-M (M: Fe, Co, Cr) alloy catalysts prepared by the polyol method in 1,2-hexadecanediol in the presence of nonanoic acid and nonylamine as protecting agents. The results of linear sweep voltammetry indicated that the Pt alloy catalysts exhibited 1.5–1.7 times higher oxygen reduction activity than that of the as-synthesized and commercial Pt catalyst. Additionally, electrocatalytic activity and stability on graphene supported Pt<sub>3</sub>-Co and Pt<sub>3</sub>-Cr alloy catalysts were reported by Rao *et al.* [150] for the oxygen reduction reaction. The fuel cell performance of the catalysts was evaluated with 0.4 mg<sub>Pt</sub> cm<sup>-2</sup> catalyst loading on the cathode and at 353 K and 1 atm. The power densities of 790, 875, 985 mW cm<sup>-2</sup> were observed for graphene supported Pt, Pt<sub>3</sub>-Co, and Pt<sub>3</sub>-Cr catalysts, respectively. The stability of the so-called catalysts were investigated by using continuous potential cyclic voltammetry swept for 500 cycles in O<sub>2</sub>-saturated 0.5 M H<sub>2</sub>SO<sub>4</sub> and then linear scan voltammetry recorded at 1600 rpm and 5 mV s<sup>-1</sup>. No obvious decrease in the oxygen reduction activity was observed for graphene supported catalysts after a continuous 500 cycles. Santiago *et al.* [149] prepared homogeneously dispersed Pt-Co bimetallic catalysts with 1.9 nm particle size, which have a high degree of alloying without thermal treatment. H<sub>2</sub>/O<sub>2</sub> PEM fuel cell polarization curves for oxygen reduction were recorded at 80 °C with a 0.4 mg cm<sup>-2</sup> total metal loading. The single cell polarization response related to the as-prepared catalysts exhibited superior mass activity compared to commercial Pt/C catalyst. As reported by

Chen and co-workers [161], shape controlled Pt-Ni bimetallic nanocrystals exhibit enhanced oxygen reduction activity. Pt<sub>3</sub>-Ni nanoframe catalysts exhibited in mass activity a factor of 22 and in specific activity a factor of 36, for the enhancement for the oxygen reduction reaction. In addition to the high intrinsic and mass activities, Pt<sub>3</sub>-Ni nanoframe catalysts showed considerable durability for a duration of 10,000 potential cycles at different scan rates from 2–200 mV s<sup>-1</sup>. Kumar *et al.* [162] prepared carbon supported palladium catalysts by using the polyol process for the oxygen reduction reaction. They reported that pretreatment of Vulcan XC-72R carbon support influenced Pd nanoparticle morphology and its activity towards the oxygen reduction reaction in acidic solution. The mass activities, measured at 0.7 V vs. RHE, for Pd at 0.07 M H<sub>3</sub>PO<sub>4</sub>, 10% H<sub>2</sub>O<sub>2</sub> and 0.2 M KOH treated carbon supports were superior to that of E-TEK 20% Pd/C. They observed less than 4% H<sub>2</sub>O<sub>2</sub> formation on different Pd/C catalysts in the kinetic potential regions. The Tafel slopes of the oxygen reduction reaction on different Pd/C catalysts showed two different regions with two different slopes. These Tafel slope values are about 60 and 120 mV dec<sup>-1</sup>, at the low current and high current density regions, suggesting different adsorption isotherms of oxygenated species such as Temkin and Langmuir isotherms [163,164], respectively. Carbon supported Pt-Cu bimetallic catalysts were prepared by the polyol process for the oxygen reduction reaction by Tseng *et al.* [155]. The prepared catalysts were exposed under 300, 600, 900 °C for 1 h in a flowing mixture of 90% Ar–10% H<sub>2</sub>. They reported that the Pt-Cu/C catalyst treated at 300 °C exhibited superior catalytic activity in terms of mass activity and specific activity than that of Pt/C in 0.1 M HClO<sub>4</sub>. From the experimental data recorded at 1600 rpm and 5 mV s<sup>-1</sup>, it was reported that Pt-Cu/C-300 showed the highest mass activity of 651 mA mg<sup>-1</sup>, and the highest specific activity of 1.33 mA cm<sup>-2</sup>. In the case of Pt-Cu/C-600 and Pt-Cu/C-900, lower mass and specific activities were observed than that of the unheated Pt-Cu/C catalyst.

As a conclusion, the polyol reduction process permits the preparation of size and shape controlled metal nanoparticles by improving the synthesis parameters for electrochemical applications. Parameters such as reaction duration, reaction temperature, and the pH value of the electrolyte assist to a remarkable extent the reduction kinetics [63,80].

### 3.3. ORR Activity on Pt/C Electrocatalyst Synthesized from BAE Method

Recently introduced in nanoscale material science, the BAE method enables the preparation of nanoscale electrocatalysts without using organic molecules. Materials from this advanced synthetic route have been primarily used as anode materials for organics electro-oxidation [36,38,101] and have been successfully utilized as anode-based electrodes in the glucose hybrid biofuel cell for bionanotechnology applications. More importantly, it has been demonstrated that Au-Pt catalysts prepared with the BAE method exhibit unexpected cathode selectivity-tolerance-durability in mixed reactants and in a poisoning environment, and physiological medium [102]. Indeed, Au<sub>60</sub>Pt<sub>40</sub> bimetallic (3.2 nm) supported onto carbon Ketjenblack EC 600-JD was able to selectively reduce oxygen in a membraneless biomedical implantable glucose fuel cell at pH 7.7 in human serum to activate a pacemaker, which constitutes a real application [102]. To some extent, BAE allows the development of advanced low temperature FCs electrocatalysts. In order to check these exceptional behaviors and compare them with the existing methods in acidic and alkaline media using the RRDE technique, we conducted ORR at 20 wt% Pt/C, as prepared from BAE as a state-of-art catalytic material [9,28,165,166]. In both media, several metal

loadings were studied ranging from 6–100  $\mu\text{g}_{\text{Pt}} \text{cm}^{-2}$ . Durability tests were performed by cycling the electrode potential from 0.05–1.10 V vs. RHE for 1000 cyclic voltammograms (CVs). Figure 12a shows the ORR polarization curves recorded in  $\text{O}_2$ -saturated 0.1 M  $\text{HClO}_4$ . Before recording these curves, the RRDE setups were calibrated as illustrated in Figure 9. Then, the electrode was scanned from 0.05–1.1 V vs. RHE at  $50 \text{ mV s}^{-1}$  twenty times followed by 2 CVs at  $5 \text{ mV s}^{-1}$ . Finally ORR was performed by scanning the disc (glassy carbon,  $0.196 \text{ cm}^2$ ) from 1.1–0.2 V vs. RHE at  $5 \text{ mV s}^{-1}$ , while that of the potential of the ring (platinum,  $0.11 \text{ cm}^2$ ) was fixed at 1.2 V vs. RHE to oxidize any peroxide intermediate. The oxygen reduction at the disc starts earlier than 1 V vs. RHE, with negligible  $\text{H}_2\text{O}_2$  in the whole scanned potential range. As a first qualitative observation, the catalyst displays good kinetics because of the sharp current behavior in the potential range of 1.0–0.8 V vs. RHE reaching a half-potential ( $E_{1/2}$ ) of 0.90 and 0.85 vs. RHE for 400 and 900 rpm, respectively. Almost the same value of the OCP and  $E_{1/2}$  were reached in 0.1 M NaOH. The important diffusion current density obtained herein and compared to that resulting in the w/o method can be assigned to the synthetic method, whereas the magnitude of the metal loading is almost two times lower [33,52]. One of the recurring themes in the FCs performance loss is the decrease of the ORR activity due to the active electrochemical surface area (ECSA) loss over the cycles [9,58,167–170]. The durability test was performed as depicted in Figure 12b. It provides evidence that the BAE method delivers prototype catalyst with impressive durability performances where the ORR curve is superimposed with the initial polarization curve, even if the catalyst loses 12% on its maximum ECSA. Indeed, compared to the current carbon supported nanoparticles, in such a situation, the catalyst is expected to lose more than 50% [58,171,172].

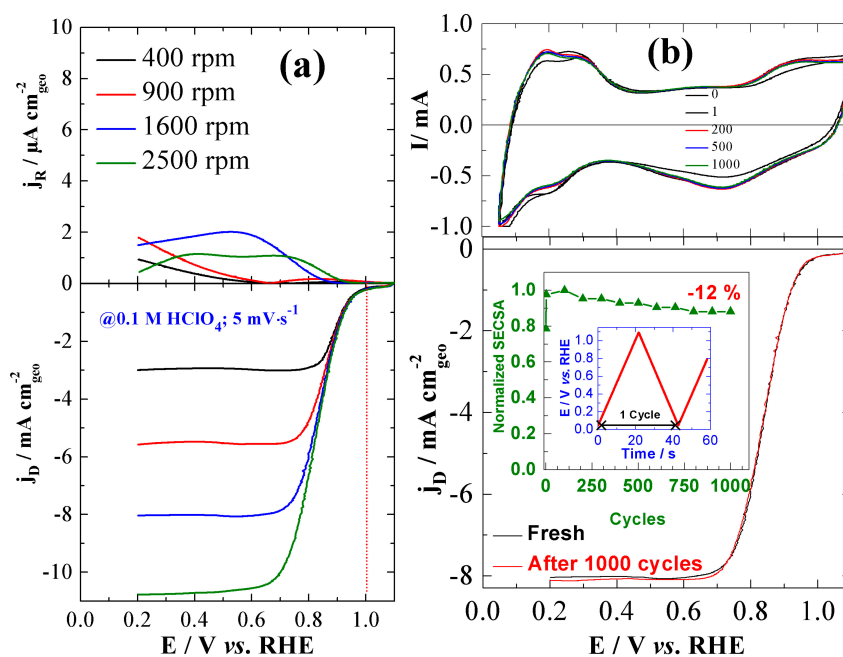


**Figure 12.** ORR polarization curves recorded in a  $\text{O}_2$ -saturated 0.1 M  $\text{HClO}_4$  solution at 20 wt% Pt/C catalyst prepared from the BAE method: (a) Ring (top) and disc (bottom) current density; (b) Electrochemical durability (top) and the ORR polarization after 1000 CVs (bottom). ORR performed at  $5 \text{ mV s}^{-1}$ , 1600 rpm, and room temperature. Insets show the SECSA decay over the 1000 cycles from 0.05–1.1 V vs. RHE at  $50 \text{ mV s}^{-1}$ . Metal loading on the electrode:  $100 \mu\text{g}_{\text{Pt}} \text{cm}^{-2}$ .

The kinetic parameters of the catalyst were analyzed. Figure 13a shows the Koutecky-Levich plots, highlighting a linear dependence at all potentials. This linearity combined with the parallelism is not surprising and clearly indicates that the oxygen reduction reaction is first-order kinetics with respect to oxygen. The type of plot is crucial for determining the apparent kinetic current density at each potential. Then, all these values are plotted as in Figure 13b to give the limiting current density ( $j_L$ ). In 0.1 M HClO<sub>4</sub>,  $j_L = 150$  and  $140 \text{ mA cm}^{-2}$  for the initial Pt/C and Pt/C after 1000 CVs, respectively. These values are found to be  $105$  and  $97 \text{ mA cm}^{-2}$  in 0.1 M NaOH. Considering the likely impact of the electrolyte on the ORR performances at the nanoparticles, Nesselberger *et al.* [5] found in 2011 that the absolute reaction rates decrease in the order HClO<sub>4</sub> > KOH > H<sub>2</sub>SO<sub>4</sub>. They explained it by the anionic adsorption strength increase (acid solutions), whereas the lower activity of KOH compared to HClO<sub>4</sub> might be due to the noncovalent interactions between hydrated K<sup>+</sup> and adsorbed OH<sup>-</sup> [5,173]. Because of the ORR improved durability and activity in HClO<sub>4</sub>, this solution is the electrolyte of choice for the electrochemical tests in a three-electrode cell [11,14,173–175].

Two Tafel slopes (inset in Figure 13b) were determined:  $125 \text{ mV dec}^{-1}$  at low overpotential (PtO<sub>x</sub> region) and  $63 \text{ mV dec}^{-1}$  at high overpotential (Pt free region). On the fresh Pt/C electrode, these values were  $130$  and  $67$ , respectively. Besides,  $126$  and  $69 \text{ mV dec}^{-1}$  were evaluated with the fresh catalyst. Then,  $140$  and  $71 \text{ mV dec}^{-1}$  were obtained after the durability test in 0.1 M NaOH. All these determined Tafel slopes are close to the theoretical ones, which are  $120 \text{ mV dec}^{-1}$  (low  $\eta$ ) and  $60 \text{ mV dec}^{-1}$  (high  $\eta$ ) [126]. It should be emphasized that these values are in agreement with those reported both for Temkin adsorption isotherms of oxygenated species (low  $\eta$ ), or Langmuir ones for high  $\eta$  (where Pt surface is free of PtO<sub>x</sub> species) [176,177].

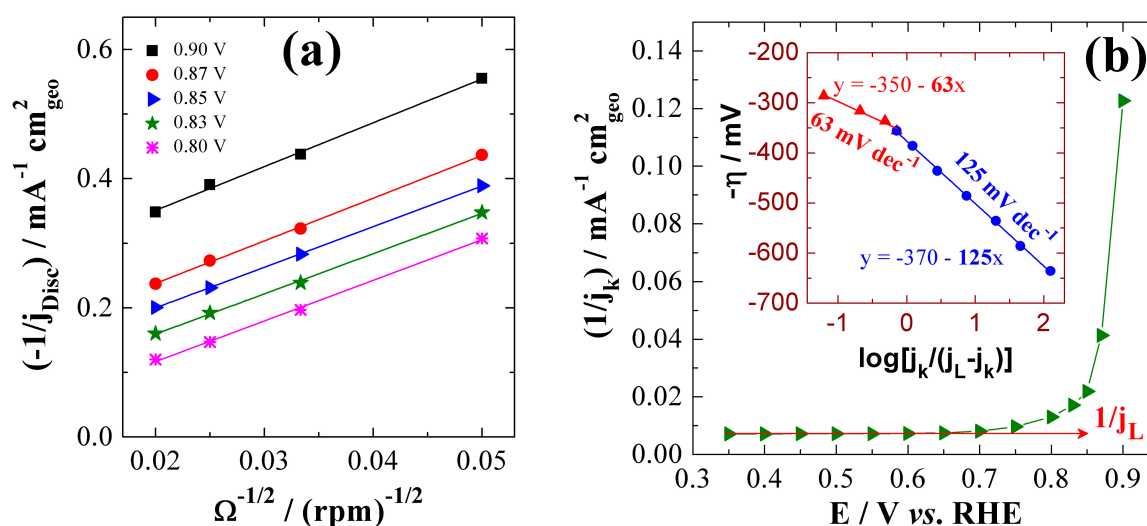
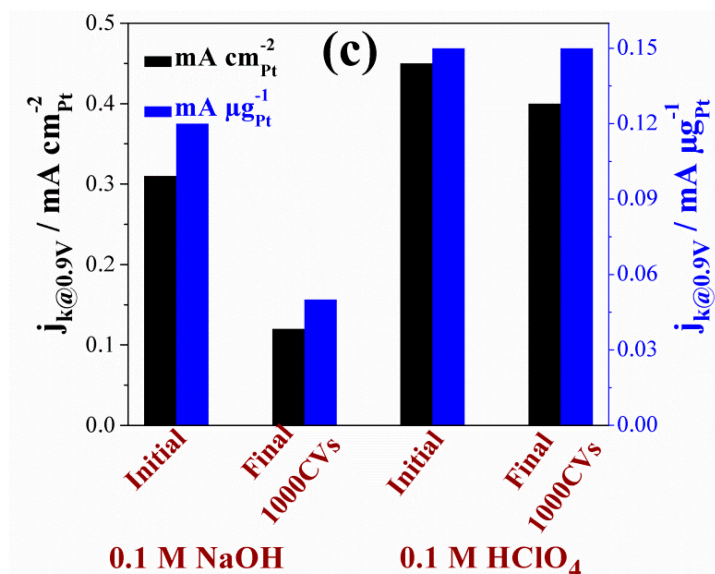


Figure 13. Cont.



**Figure 13.** (a) Koutecky–Levich and (b)  $j_k^{-1}$  plot for the determination of  $j_L$ . Inset in (b) shows the Tafel plots: data are extracted from ORR after the durability test in 0.1 M HClO<sub>4</sub>. (c) Comparison of  $j_k$  at 0.9 V vs. RHE in 0.1 M HClO<sub>4</sub> and 0.1 M NaOH.

Figure 13c gathers the kinetic current (extracted from Figure 13a) normalized either with ECSA mass ( $\text{mA cm}^{-2}_{\text{Pt}}$ ) or Pt mass ( $\text{mA } \mu\text{g}^{-1}_{\text{Pt}}$ ) at 0.9 V vs. RHE. Initially,  $j_k = 0.45 \text{ mA cm}^{-2}_{\text{Pt}}$  ( $0.15 \text{ mA } \mu\text{g}^{-1}_{\text{Pt}}$ ) in 0.1 M HClO<sub>4</sub> and  $j_k = 0.31 \text{ mA cm}^{-2}_{\text{Pt}}$  ( $0.12 \text{ mA } \mu\text{g}^{-1}_{\text{Pt}}$ ) in 0.1 M NaOH. After the durability test, they became  $j_k = 0.40 \text{ mA cm}^{-2}_{\text{Pt}}$  ( $0.15 \text{ mA } \mu\text{g}^{-1}_{\text{Pt}}$ ) in 0.1 M HClO<sub>4</sub> and  $j_k = 0.14 \text{ mA cm}^{-2}_{\text{Pt}}$  ( $0.05 \text{ mA } \mu\text{g}^{-1}_{\text{Pt}}$ ) in 0.1 M NaOH, meaning a good stability in acid medium and a performance loss in the alkaline medium. The stability could be improved by the addition of second metals like palladium or gold to platinum. Table 1 summarizes the different parameters. It can be seen that  $j_0$  is  $179 \cdot 10^{-3} \text{ mA cm}^{-2}$  (and  $153 \cdot 10^{-3} \text{ mA cm}^{-2}$  after stability) in HClO<sub>4</sub>, and  $122 \cdot 10^{-3} \text{ mA cm}^{-2}$  (and  $114 \cdot 10^{-3} \text{ mA cm}^{-2}$  after stability) in NaOH, respectively. These values of  $j_0$  are more important than those reported by Demarconnay *et al.* [33] ( $16.8 \text{ mA cm}^{-2}$ ) and Habrioux *et al.* [52] ( $0.3 \cdot 10^{-3} \text{ mA cm}^{-2}$ ) on Pt/C synthesized from the w/o method, reflecting an enhanced ORR kinetics at these electrode materials.

Table 1 gathers the experimental data concerning the ORR on carbon-supported nanomaterials prepared from the colloidal method. It would be interesting to discuss each point depending on the used method. Unfortunately, there is missing information in the literature. The ORR occurs with high OCP close to 1 V vs. RHE and suitable half-potential ( $E_{1/2}$ ) roughly at 0.85 V vs. RHE, as on the most active and advanced Vulcan supported PtCo [3,14], PtNi [3,11] or PtNiCo [13] nanoparticles as well as on the free nanoparticles in solution (unsupported catalysts) [10,65]. The other interesting result from this table concerns the number of exchanged electrons. This value is close to 4, which means that the reaction does not produce any significant peroxide, maximizing the Faradaic yield. Conversely, it is difficult to compare the kinetic activity with  $j_k$  due to the fact that some authors did not clearly indicate whether the current was normalized with the geometric or active surface area. For this, we recommend further papers include full information concerning their materials for better comparison.

**Table 1.** Comparative performances of oxygen reduction reaction (ORR) results from RRDE experiments on various catalysts prepared from colloidal methods.  $E_{1/2}$  was graphically determined at 1600 rpm (potential at  $i = I_D/2$ ). Note: OCP, “w/o” and “BAE” refer to open circuit potential, water-in-oil and bromide anion exchange methods, respectively. Empty box (–) means that the original article does not provide such data.

Catalyst	Electrolyte	OCP	$E_{1/2}$	$j_k$ ( $\text{mA cm}^{-2}_{\text{Pt}}$ )		Tafel slope ( $\text{mV dec}^{-1}$ )		$j_0$ ( $\times 10^{-3} \text{ mA cm}^{-2}$ )		$n_{\text{ex}}$	Method And Ref.
				At		Low	High	Low	High		
				V vs. RHE							
50 wt% Pt/C	0.2 M NaOH	1.05	0.85	0.60	-	81	126	1.2	16.8	4	w/o [33]
50 wt% Pt <sub>80</sub> Bi <sub>20</sub> /C		1.05	0.87	1.14	-	62	127	0.3	23.2	4	
20 wt% Pd/C	1 M NaOH	0.95	0.83	-	0.07	89	162	-	11.1	3.9	w/o [56]
20 wt% Pd <sub>70</sub> Ni <sub>30</sub> /C		0.95	0.85	-	0.06	76	133	-	1.63	3.8	
20 wt% Pd/C	0.5 M H <sub>2</sub> SO <sub>4</sub>	0.80	0.70	-	-	60	120	-	-	4	Polyol [162]
20 wt% Pt/C		0.925	0.84	-	-	-	-	-	-	4	Polyol [152]
20 wt% Pt-Co/C		0.980	0.85	-	-	-	-	-	-	4	Polyol [152]
20 wt% Pt-Cr/C		0.985	0.85	-	-	-	-	-	-	4	Polyol [152]
20 wt% Ag/C	0.1 M NaOH	0.95	0.80	-	-	-	6.3	-	157	3.9	w/o [178]
20 wt% Pt/C	0.1 M HClO <sub>4</sub>	1.09	0.85	0.45	1.01	67	130	0.45	179	4.0	BAE Here
	0.1 M NaOH	1.08	0.85	0.31	0.77	69	126	0.64	122	4.0	

#### 4. Summary and Perspectives

This review paper focused on the preparation and application of carbon supported nanoparticles in electrocatalysis, and especially on the oxygen reduction reaction (ORR) in low temperature fuel cells (FCs). We examined the recent developments in nanocatalysts preparation science in order to better understand and correlate their catalytic performances toward the ORR. From this survey, we found that the catalytic properties can be precisely and effectively tuned by changing the experimental conditions. Definitely, among the developed methods for carbon-supported nanoparticles, the colloidal ones are the most used in ORR electrochemistry. The state-of-the-art Pt/C electrocatalyst shows poor long-term stability and different co-atoms (Co, Ni, Bi, Ag, Au) have been proposed to improve its performances. The reaction on Pt-based electrodes starts at *ca.* 1.1 V vs. RHE, which represents only 100 mV difference compared to the theoretical value (close to 1.2 V vs. RHE). More importantly, most of the

optimized systems, display sharp behavior between 0.8–0.9 V vs. RHE in the potential-current ORR polarization curves, for the range of interest for FCs applications. From the different results, it can be concluded that the oxygen reduction reaction at the metal nanoparticles depends strongly on the electrolyte medium as well as the particle size. Fundamental studies at the laboratory scale reveal that the reaction kinetics decreases in the order  $\text{HClO}_4 > \text{NaOH}$  (or  $\text{KOH}$ )  $> \text{H}_2\text{SO}_4$ . For the particles size effect, the optimum window is 2–3 nm, where the active sites on the corners and edges are more available. Unfortunately, basic but fundamental data are missing in research papers about the kinetic parameters to enable better comparison. In this review paper, we were not able to compare the specific kinetics of the different electrode materials derived from the various preparation methods due to lack of information. Future studies are urged to provide clear and full in depth information on their ORR tests.

These recent advances in low temperature FCs electrocatalysts preparation indicate that the standard and quality of fundamental research in this area needs to continue unabated. Water-in-oil has been the method of choice for heterogeneous catalysis. The inability to clean the nanoparticles surface from the organic molecules used as surfactant affects the catalytic performance of the obtained catalysts. The recent initiated “Bromide Anion Exchange, BAE” method leads to various surfactant-free nanoparticles. Undoubtedly, the performance of such materials in the long term is expected to be of particular importance in fuel cell science. Even catalysts from colloidal methods (water-in-oil, polyol, Bönemann, BAE) have demonstrated excellent ability toward the ORR; they have not been widely tested in the Membrane-Electrode-Assembly, MEA. Future works in this area should first focus on the performances of carbon supported metal nanoparticles in MEAs for the *in situ* oxygen reduction reaction as well as the FC results. Furthermore, in order to reduce the electrode cost and thus the FC system, incorporating non-noble metals is needed to reduce the amount of precious metals in the electrode materials. The experimental tools provided herein will be useful for early career researchers in FCs and could help in finding suitable ORR methodology.

### Acknowledgments

The authors would like to thank financial supports from the French National Research Agency (ANR) through the program “ChemBio-Energy” and “Region Poitou-Charentes”.

### Author Contributions

Kouakou B. Kokoh conceived the project. Yaovi Holade and Nihat Ege Sahin wrote the first draft of the manuscript which was then improved by Karine Servat, Teko W. Napporn and Kouakou B. Kokoh. All the authors researched the literature.

### Conflicts of Interest

The authors declare no conflict of interest.

## References

1. Marković, N.M.; Ross, P.N., Jr. Surface science studies of model fuel cell electrocatalysts. *Surf. Sci. Rep.* **2002**, *45*, 117–229.
2. Wieckowski, A.; Savinova, E.R.; Vayenas, C.G. *Catalysis and Electrocatalysis at Nanoparticle Surfaces*; Marcel Dekker, Inc.: New York, NY, USA, 2003; p. 970.
3. Stamenkovic, V.R.; Mun, B.S.; Arenz, M.; Mayrhofer, K.J.J.; Lucas, C.A.; Wang, G.; Ross, P.N.; Markovic, N.M. Trends in electrocatalysis on extended and nanoscale Pt-bimetallic alloy surfaces. *Nat. Mater.* **2007**, *6*, 241–247.
4. Markovic, N.M.; Gasteiger, H.A.; Ross, P.N. Oxygen Reduction on Platinum Low-Index Single-Crystal Surfaces in Sulfuric Acid Solution: Rotating Ring-Pt(hkl) Disk Studies. *J. Phys. Chem.* **1995**, *99*, 3411–3415.
5. Nesselberger, M.; Ashton, S.; Meier, J.C.; Katsounaros, I.; Mayrhofer, K.J.J.; Arenz, M. The Particle Size Effect on the Oxygen Reduction Reaction Activity of Pt Catalysts: Influence of Electrolyte and Relation to Single Crystal Models. *J. Am. Chem. Soc.* **2011**, *133*, 17428–17433.
6. Shao, M.; Peles, A.; Shoemaker, K. Electrocatalysis on Platinum Nanoparticles: Particle Size Effect on Oxygen Reduction Reaction Activity. *Nano Lett.* **2011**, *11*, 3714–3719.
7. Anastasopoulos, A.; Davies, J.C.; Hannah, L.; Hayden, B.E.; Lee, C.E.; Milhano, C.; Mormiche, C.; Offin, L. The Particle Size Dependence of the Oxygen Reduction Reaction for Carbon-Supported Platinum and Palladium. *ChemSusChem* **2013**, *6*, 1973–1982.
8. Hernandez-Fernandez, P.; Masini, F.; McCarthy, D.N.; Strebel, C.E.; Friebel, D.; Deiana, D.; Malacrida, P.; Nierhoff, A.; Bodin, A.; Wise, A.M.; *et al.* Mass-selected nanoparticles of Pt<sub>x</sub>Y as model catalysts for oxygen electroreduction. *Nat. Chem.* **2014**, *6*, 732–738.
9. Debe, M.K. Electrocatalyst approaches and challenges for automotive fuel cells. *Nature* **2012**, *486*, 43–51.
10. Cui, C.; Gan, L.; Li, H.-H.; Yu, S.-H.; Heggen, M.; Strasser, P. Octahedral PtNi Nanoparticle Catalysts: Exceptional Oxygen Reduction Activity by Tuning the Alloy Particle Surface Composition. *Nano Lett.* **2012**, *12*, 5885–5889.
11. Chen, C.; Kang, Y.; Huo, Z.; Zhu, Z.; Huang, W.; Xin, H.L.; Snyder, J.D.; Li, D.; Herron, J.A.; Mavrikakis, M.; *et al.* Highly Crystalline Multimetallic Nanoframes with Three-Dimensional Electrocatalytic Surfaces. *Science* **2014**, *343*, 1339–1343.
12. Corti, H.; Gonzalez, E.R. *Direct Alcohol Fuel Cells: Materials, Performance, Durability and Applications*; Springer: Dordrecht, The Netherlands, 2014; p. 370.
13. Huang, X.; Zhao, Z.; Chen, Y.; Zhu, E.; Li, M.; Duan, X.; Huang, Y. A Rational Design of Carbon-Supported Dispersive Pt-Based Octahedra as Efficient Oxygen Reduction Reaction Catalysts. *Energy Environ. Sci.* **2014**, *7*, 2957–2962.
14. Wang, D.; Xin, H.L.; Hovden, R.; Wang, H.; Yu, Y.; Muller, D.A.; DiSalvo, F.J.; Abruña, H.D. Structurally ordered intermetallic platinum–cobalt core–shell nanoparticles with enhanced activity and stability as oxygen reduction electrocatalysts. *Nat. Mater.* **2013**, *12*, 81–87.

15. Ross, P.N.; Radmilovic, V.; Markovic, N.M. Physical and Electrochemical Characterization of Bimetallic Nanoparticle Electrocatalysts. In *Catalysis and Electrocatalysis at Nanoparticle Surfaces*; Wieckowski, A., Savinova, E.R., Vayenas, C.G., Eds.; CRC Press: New York, NY, USA, 2003; pp. 311–342.
16. Geim, A.K.; Novoselov, K.S. The rise of graphene. *Nat. Mater.* **2007**, *6*, 183–191.
17. De Volder, M.F. L.; Tawfick, S.H.; Baughman, R.H.; Hart, A.J. Carbon Nanotubes: Present and Future Commercial Applications. *Science* **2013**, *339*, 535–539.
18. Andrews, R.; Jacques, D.; Qian, D.; Rantell, T. Multiwall Carbon Nanotubes: Synthesis and Application. *Acc. Chem. Res.* **2002**, *35*, 1008–1017.
19. Karousis, N.; Tagmatarchis, N.; Tasis, D. Current Progress on the Chemical Modification of Carbon Nanotubes. *Chem. Rev.* **2010**, *110*, 5366–5397.
20. Che, A.-F.; Germain, V.; Cretin, M.; Cornu, D.; Innocent, C.; Tingry, S. Fabrication of free-standing electrospun carbon nanofibers as efficient electrode materials for bioelectrocatalysis. *New J. Chem.* **2011**, *35*, 2848–2853.
21. Andersen, S.M.; Borghei, M.; Lund, P.; Elina, Y.-R.; Pasanen, A.; Kauppinen, E.; Ruiz, V.; Kauranen, P.; Skou, E.M. Durability of carbon nanofiber (CNF) & carbon nanotube (CNT) as catalyst support for Proton Exchange Membrane Fuel Cells. *Solid State Ionics* **2013**, *231*, 94–101.
22. Shulaker, M.M.; Hills, G.; Patil, N.; Wei, H.; Chen, H.-Y.; Wong, H.S.P.; Mitra, S. Carbon nanotube computer. *Nature* **2013**, *501*, 526–530.
23. Gao, F.; Viry, L.; Maugey, M.; Poulin, P.; Mano, N. Engineering hybrid nanotube wires for high-power biofuel cells. *Nat. Commun.* **2010**, *1*, 3.
24. Zebda, A.; Gondran, C.; le Goff, A.; Holzinger, M.; Cinquin, P.; Cosnier, S. Mediatorless high-power glucose biofuel cells based on compressed carbon nanotube-enzyme electrodes. *Nat. Commun.* **2011**, *2*, 370.
25. Sinfelt, J.H.; Lam, Y.L.; Cusumano, J.A.; Barnett, A.E. Nature of ruthenium-copper catalysts. *J. Catal.* **1976**, *42*, 227–237.
26. Ferrando, R.; Jellinek, J.; Johnston, R.L. Nanoalloys: From Theory to Applications of Alloy Clusters and Nanoparticles. *Chem. Rev.* **2008**, *108*, 845–910.
27. Raimondi, F.; Scherer, G.G.; Kötz, R.; Wokaun, A. Nanoparticles in Energy Technology: Examples from Electrochemistry and Catalysis. *Angew. Chem. Int. Ed.* **2005**, *44*, 2190–2209.
28. Katsounaros, I.; Cherevko, S.; Zeradjanin, A.R.; Mayrhofer, K.J.J. Oxygen Electrochemistry as a Cornerstone for Sustainable Energy Conversion. *Angew. Chem. Int. Ed.* **2014**, *53*, 102–121.
29. Hoar, T.; Schulman, J. Transparent water-in-oil dispersions: the oleopathic hydro-micelle. *Nature* **1943**, *152*, 102–103.
30. Boutonnet, M.; Kizling, J.; Stenius, P.; Maire, G. The preparation of monodisperse colloidal metal particles from microemulsions. *Colloids Surf.* **1982**, *5*, 209–225.
31. Schwuger, M.-J.; Stickdorn, K.; Schomaecker, R. Microemulsions in Technical Processes. *Chem. Rev.* **1995**, *95*, 849–864.
32. Bock, C.; Halvorsen, H.; MacDougall, B. Catalyst Synthesis Techniques. In *PEM Fuel Cell Electrocatalysts and Catalyst Layers*; Zhang, J., Ed.; Springer-Verlag: London, UK, 2008; pp. 447–485.

33. Demarconnay, L.; Coutanceau, C.; Léger, J.M. Study of the oxygen electroreduction at nanostructured PtBi catalysts in alkaline medium. *Electrochim. Acta* **2008**, *53*, 3232–3241.
34. Simões, M.; Baranton, S.; Coutanceau, C. Electrooxidation of Sodium Borohydride at Pd, Au, and Pd<sub>x</sub>Au<sub>1-x</sub> Carbon-Supported Nanocatalysts. *J. Phys. Chem. C* **2009**, *113*, 13369–13376.
35. Roychowdhury, C.; Matsumoto, F.; Mutolo, P.F.; Abruña, H.D.; DiSalvo, F.J. Synthesis, Characterization, and Electrocatalytic Activity of PtBi Nanoparticles Prepared by the Polyol Process. *Chem. Mater.* **2005**, *17*, 5871–5876.
36. Holade, Y.; Morais, C.; Arrii-Clacens, S.; Servat, K.; Napporn, T.W.; Kokoh, K.B. New Preparation of PdNi/C and PdAg/C Nanocatalysts for Glycerol Electrooxidation in Alkaline Medium. *Electrocatalysis* **2013**, *4*, 167–178.
37. Holade, Y.; Morais, C.; Napporn, T.W.; Servat, K.; Kokoh, K.B. Electrochemical Behavior of Organics Oxidation on Palladium-Based Nanocatalysts Synthesized from Bromide Anion Exchange. *ECS Trans.* **2014**, *58*, 25–35.
38. Tonda-Mikiela, P.; Napporn, T.W.; Morais, C.; Servat, K.; Chen, A.; Kokoh, K.B. Synthesis of Gold-Platinum Nanomaterials Using Bromide Anion Exchange-Synergistic Electroactivity toward CO and Glucose Oxidation. *J. Electrochem. Soc.* **2012**, *159*, H828–H833.
39. Lahmani, M.; Bréchnignac, C.; Houdy, P. *Les Nanosciences: 2. Nanomatériaux et Nanochimie*; 2nd ed.; Belin: Paris, France, 2012, p. 732 (In French).
40. Schulman, J.H.; Stoeckenius, W.; Prince, L.M. Mechanism of Formation and Structure of Micro Emulsions by Electron Microscopy. *J. Phys. Chem.* **1959**, *63*, 1677–1680.
41. Schulman, J.H.; Friend, J.A. Light scattering investigation of the structure of transparent oil-water disperse systems. II. *J. Colloid Sci.* **1949**, *4*, 497–509.
42. Clause, M.; Peyrelasse, J.; Heil, J.; Boned, C.; Lagourette, B. Bicontinuous structure zones in microemulsions. *Nature* **1981**, *293*, 636–638.
43. Danielsson, I.; Lindman, B. The definition of microemulsion. *Colloids Surf.* **1981**, *3*, 391–392.
44. Eriksson, S.; Nylén, U.; Rojas, S.; Boutonnet, M. Preparation of catalysts from microemulsions and their applications in heterogeneous catalysis. *Appl. Catal. A* **2004**, *265*, 207–219.
45. Capek, I. Preparation of metal nanoparticles in water-in-oil (w/o) microemulsions. *Adv. Colloid Int. Sci.* **2004**, *110*, 49–74.
46. Ingelsten, H.H.; Bagwe, R.; Palmqvist, A.; Skoglundh, M.; Svanberg, C.; Holmberg, K.; Shah, D.O. Kinetics of the Formation of Nano-Sized Platinum Particles in Water-in-Oil Microemulsions. *J. Colloid Int. Sci.* **2001**, *241*, 104–111.
47. Solla-Gullón, J.; Rodes, A.; Montiel, V.; Aldaz, A.; Clavilier, J. Electrochemical characterisation of platinum–palladium nanoparticles prepared in a water-in-oil microemulsion. *J. Electroanal. Chem.* **2003**, *554–555*, 273–284.
48. Solla-Gullón, J.; Vidal-Iglesias, F.J.; Montiel, V.; Aldaz, A. Electrochemical characterization of platinum–ruthenium nanoparticles prepared by water-in-oil microemulsion. *Electrochim. Acta* **2004**, *49*, 5079–5088.
49. Habrioux, A. Préparation et caractérisation de nanoparticules à base d’or et de platine pour l’anode d’une biopile glucose/dioxygène. Ph.D. Thesis, University of Poitiers, France, October 2009.

50. Simões, M. Développement d'électrocatalyseurs anodiques plurimétalliques nanostructurés pour une application en pile à combustible à membrane alcaline solide (SAMFC). Ph.D. Thesis, University of Poitiers, France, March 2011.
51. Liu, H.; Song, C.; Zhang, L.; Zhang, J.; Wang, H.; Wilkinson, D.P. A review of anode catalysis in the direct methanol fuel cell. *J. Power Sources* **2006**, *155*, 95–110.
52. Habrioux, A.; Diabaté, D.; Rousseau, J.; Napporn, T.; Servat, K.; Guétaz, L.; Trokourey, A.; Kokoh, K.B. Electrocatalytic Activity of Supported Au–Pt Nanoparticles for CO Oxidation and O<sub>2</sub> Reduction in Alkaline Medium. *Electrocatalysis* **2010**, *1*, 51–59.
53. Habrioux, A.; Sibert, E.; Servat, K.; Vogel, W.; Kokoh, K.B.; Alonso-Vante, N. Activity of Platinum–Gold Alloys for Glucose Electrooxidation in Biofuel Cells. *J. Phys. Chem. B* **2007**, *111*, 10329–10333.
54. Habrioux, A.; Vogel, W.; Guinel, M.; Guetaz, L.; Servat, K.; Kokoh, B.; Alonso-Vante, N. Structural and electrochemical studies of Au-Pt nanoalloys. *Phys. Chem. Chem. Phys.* **2009**, *11*, 3573–3579.
55. Wu, M.-L.; Chen, D.-H.; Huang, T.-C. Preparation of Au/Pt Bimetallic Nanoparticles in Water-in-Oil Microemulsions. *Chem. Mater.* **2001**, *13*, 599–606.
56. Diabaté, D.; Napporn, T.W.; Servat, K.; Habrioux, A.; Arrii-Clacens, S.; Trokourey, A.; Kokoh, K.B. Kinetic Study of Oxygen Reduction Reaction on Carbon Supported Pd-Based Nanomaterials in Alkaline Medium. *J. Electrochem. Soc.* **2013**, *160*, H302–H308.
57. Holade, Y.; Morais, C.; Servat, K.; Napporn, T.W.; Kokoh, K.B. Enhancing the available specific surface area of carbon supports to boost the electroactivity of nanostructured Pt catalysts. *Phys. Chem. Chem. Phys.* **2014**, *16*, 25609–25620.
58. Grolleau, C.; Coutanceau, C.; Pierre, F.; Léger, J.M. Effect of potential cycling on structure and activity of Pt nanoparticles dispersed on different carbon supports. *Electrochim. Acta* **2008**, *53*, 7157–7165.
59. Solla-Gullón, J.; Montiel, V.; Aldaz, A.; Clavilier, J. Electrochemical characterisation of platinum nanoparticles prepared by microemulsion: How to clean them without loss of crystalline surface structure. *J. Electroanal. Chem.* **2000**, *491*, 69–77.
60. Napporn, T.; Habrioux, A.; Rousseau, J.; Servat, K.; Léger, J.-M.; Kokoh, B. Effect of the Cleaning Step on the Morphology of Gold Nanoparticles. *Electrocatalysis* **2011**, *2*, 24–27.
61. Fievet, F.; Lagier, J.P.; Blin, B.; Beaudoin, B.; Figlarz, M. Homogeneous and heterogeneous nucleations in the polyol process for the preparation of micron and submicron size metal particles. *Solid State Ionics* **1989**, *32–33* (Part 1), 198–205.
62. Bonet, F.; Guéry, C.; Guyomard, D.; Herrera Urbina, R.; Tekaiia-Elhissen, K.; Tarascon, J.M. Electrochemical reduction of noble metal compounds in ethylene glycol. *Int. J. Inorg. Mater.* **1999**, *1*, 47–51.
63. Bock, C.; Paquet, C.; Couillard, M.; Botton, G.A.; MacDougall, B.R. Size-Selected Synthesis of PtRu Nano-Catalysts: Reaction and Size Control Mechanism. *J. Am. Chem. Soc.* **2004**, *126*, 8028–8037.
64. Skrabalak, S.E.; Wiley, B.J.; Kim, M.; Formo, E.V.; Xia, Y. On the Polyol Synthesis of Silver Nanostructures: Glycolaldehyde as a Reducing Agent. *Nano Lett.* **2008**, *8*, 2077–2081.

65. Chen, J.; Lim, B.; Lee, E.P.; Xia, Y. Shape-controlled synthesis of platinum nanocrystals for catalytic and electrocatalytic applications. *Nano Today* **2009**, *4*, 81–95.
66. Xiong, Y.; Xia, Y. Shape-Controlled Synthesis of Metal Nanostructures: The Case of Palladium. *Adv. Mater.* **2007**, *19*, 3385–3391.
67. Grzelczak, M.; Perez-Juste, J.; Mulvaney, P.; Liz-Marzan, L.M. Shape control in gold nanoparticle synthesis. *Chem. Soc. Rev.* **2008**, *37*, 1783–1791.
68. Wang, C.; Daimon, H.; Onodera, T.; Koda, T.; Sun, S. A General Approach to the Size- and Shape-Controlled Synthesis of Platinum Nanoparticles and Their Catalytic Reduction of Oxygen. *Angew. Chem. Int. Ed.* **2008**, *47*, 3588–3591.
69. Alia, S.M.; Zhang, G.; Kisailus, D.; Li, D.; Gu, S.; Jensen, K.; Yan, Y. Porous Platinum Nanotubes for Oxygen Reduction and Methanol Oxidation Reactions. *Adv. Funct. Mater.* **2010**, *20*, 3742–3746.
70. Lee, I.; Delbecq, F.; Morales, R.; Albitzer, M.A.; Zaera, F. Tuning selectivity in catalysis by controlling particle shape. *Nat. Mater.* **2009**, *8*, 132–138.
71. Kyriakou, G.; Beaumont, S.K.; Humphrey, S.M.; Antonetti, C.; Lambert, R.M. Sonogashira Coupling Catalyzed by Gold Nanoparticles: Does Homogeneous or Heterogeneous Catalysis Dominate? *ChemCatChem* **2010**, *2*, 1444–1449.
72. Campbell, C.T.; Parker, S.C.; Starr, D.E. The Effect of Size-Dependent Nanoparticle Energetics on Catalyst Sintering. *Science* **2002**, *298*, 811–814.
73. Biacchi, A.J.; Schaak, R.E. The Solvent Matters: Kinetic *versus* Thermodynamic Shape Control in the Polyol Synthesis of Rhodium Nanoparticles. *ACS Nano* **2011**, *5*, 8089–8099.
74. Song, H.; Kim, F.; Connor, S.; Somorjai, G.A.; Yang, P. Pt Nanocrystals: Shape Control and Langmuir–Blodgett Monolayer Formation. *J. Phys. Chem. B* **2004**, *109*, 188–193.
75. Susut, C.; Nguyen, T.D.; Chapman, G.B.; Tong, Y. Particle Size Limit for Concomitant Tuning of Size and Shape of Platinum Nanoparticles. *J. Cluster Sci.* **2007**, *18*, 773–780.
76. Lee, E.; Murthy, A.; Manthiram, A. Comparison of the stabilities and activities of Pt–Ru/C and Pt<sub>3</sub>–Sn/C electrocatalysts synthesized by the polyol method for methanol electro-oxidation reaction. *J. Electroanal. Chem.* **2011**, *659*, 168–175.
77. Kim, H.J.; Choi, S.M.; Green, S.; Tompsett, G.A.; Lee, S.H.; Huber, G.W.; Kim, W.B. Highly active and stable PtRuSn/C catalyst for electrooxidations of ethylene glycol and glycerol. *Appl. Catal. B: Env.* **2011**, *101*, 366–375.
78. Wang, L.; Zhai, J.-J.; Jiang, K.; Wang, J.-Q.; Cai, W.-B. Pd–Cu/C electrocatalysts synthesized by one-pot polyol reduction toward formic acid oxidation: Structural characterization and electrocatalytic performance. *Int. J. Hydrogen Energ.* **2015**, *40*, 1726–1734.
79. Wang, G.; Takeguchi, T.; Muhamad, E.N.; Yamanaka, T.; Sadakane, M.; Ueda, W. Preparation of Well-Alloyed PtRu/C Catalyst by Sequential Mixing of the Precursors in a Polyol Method. *J. Electrochem. Soc.* **2009**, *156*, B1348.
80. Joseyphus, R.J.; Matsumoto, T.; Takahashi, H.; Kodama, D.; Tohji, K.; Jeyadevan, B. Designed synthesis of cobalt and its alloys by polyol process. *J. Solid State Chem.* **2007**, *180*, 3008–3018.
81. Susut, C.; Tong, Y.J. Size-Dependent Methanol Electro-oxidation Activity of Pt Nanoparticles with Different Shapes. *Electrocatalysis* **2011**, *2*, 75–81.

82. González-Quijano, D.; Pech-Rodríguez, W.J.; Escalante-García, J.I.; Vargas-Gutiérrez, G.; Rodríguez-Varela, F.J. Electrocatalysts for ethanol and ethylene glycol oxidation reactions. Part I: Effects of the polyol synthesis conditions on the characteristics and catalytic activity of Pt–Sn/C anodes. *Int. J. Hydrogen Energ.* **2014**, *39*, 16676–16685.
83. Jiang, L.; Hsu, A.; Chu, D.; Chen, R. Ethanol electro-oxidation on Pt/C and PtSn/C catalysts in alkaline and acid solutions. *Int. J. Hydrogen Energy* **2010**, *35*, 365–372.
84. Lee, S.; Kim, H.J.; Choi, S.M.; Seo, M.H.; Kim, W.B. The promotional effect of Ni on bimetallic PtNi/C catalysts for glycerol electrooxidation. *Appl. Catal. A* **2012**, *429–430*, 39–47.
85. Nghia, N.V.; Truong, N.N.K.; Thong, N.M.; Hung, N.P. Synthesis of Nanowire-Shaped Silver by Polyol Process of Sodium Chloride. *Int. J. Mater. Chem.* **2012**, *2*, 75–78.
86. Chee, S.-S.; Lee, J.-H. Synthesis of tin nanoparticles through modified polyol process and effects of centrifuging and drying on nanoparticles. *Trans. Nonferrous Met. Soc. China* **2012**, *22*, s707–s711.
87. Salgado, J.R.C.; Antolini, E.; Gonzalez, E.R. Structure and Activity of Carbon-Supported Pt–Co Electrocatalysts for Oxygen Reduction. *J. Phys. Chem. B* **2004**, *108*, 17767–17774.
88. Alvarez, G.F.; Mamlouk, M.; Senthil Kumar, S.M.; Scott, K. Preparation and characterisation of carbon-supported palladium nanoparticles for oxygen reduction in low temperature PEM fuel cells. *J. Appl. Electrochem.* **2011**, *41*, 925–937.
89. Pradeep, T.; Anshup. Noble metal nanoparticles for water purification: A critical review. *Thin Solid Films* **2009**, *517*, 6441–6478.
90. Nashner, M.S.; Frenkel, A.I.; Somerville, D.; Hills, C.W.; Shapley, J.R.; Nuzzo, R.G. Core Shell Inversion during Nucleation and Growth of Bimetallic Pt/Ru Nanoparticles. *J. Am. Chem. Soc.* **1998**, *120*, 8093–8101.
91. Takasu, Y.; Fujiwara, T.; Murakami, Y.; Sasaki, K.; Oguri, M.; Asaki, T.; Sugimoto, W. Effect of Structure of Carbon-Supported PtRu Electrocatalysts on the Electrochemical Oxidation of Methanol. *J. Electrochem. Soc.* **2000**, *147*, 4421–4427.
92. Rahsepar, M.; Pakshir, M.; Piao, Y.; Kim, H. Preparation of Highly Active 40 wt.% Pt on Multiwalled Carbon Nanotube by Improved Impregnation Method for Fuel Cell Applications. *Fuel Cells* **2012**, *12*, 827–834.
93. Knani, S.; Chirchi, L.; Baranton, S.; Napporn, T.W.; Léger, J.-M.; Ghorbel, A. A methanol-Tolerant carbon supported Pt–Sn cathode catalysts. *Int. J. Hydrogen Energy* **2014**, *39*, 9070–9079.
94. Coutanceau, C.; Brimaud, S.; Lamy, C.; Léger, J.M.; Dubau, L.; Rousseau, S.; Vigier, F. Review of different methods for developing nanoelectrocatalysts for the oxidation of organic compounds. *Electrochim. Acta* **2008**, *53*, 6865–6880.
95. Knani, S.; Chirchi, L.; Napporn, W.T.; Baranton, S.; Léger, J.M.; Ghorbel, A. Promising ternary Pt–Co–Sn catalyst for the oxygen reduction reaction. *J. Electroanal. Chem.* **2015**, *738*, 145–153.
96. Miller, H.A.; Bevilacqua, M.; Filippi, J.; Lavacchi, A.; Marchionni, A.; Marelli, M.; Moneti, S.; Oberhauser, W.; Vesselli, E.; Innocenti, M.; *et al.* Nanostructured Fe–Ag electrocatalysts for the oxygen reduction reaction in alkaline media. *J. Mater. Chem. A* **2013**, *1*, 13337–13347.
97. Choi, S.M.; Yoon, J.S.; Kim, H.J.; Nam, S.H.; Seo, M.H.; Kim, W.B. Electrochemical benzene hydrogenation using PtRhM/C (M = W, Pd, or Mo) electrocatalysts over a polymer electrolyte fuel cell system. *Appl. Catal. A* **2009**, *359*, 136–143.

98. Kim, H.J.; Choi, S.M.; Nam, S.H.; Seo, M.H.; Kim, W.B. Effect of Rh content on carbon-supported PtRh catalysts for dehydrogenative electrooxidation of cyclohexane to benzene over polymer electrolyte membrane fuel cell. *Appl. Catal. A* **2009**, *352*, 145–151.
99. Kim, H.J.; Choi, S.M.; Nam, S.H.; Seo, M.H.; Kim, W.B. Carbon-supported PtNi catalysts for electrooxidation of cyclohexane to benzene over polymer electrolyte fuel cells. *Catal. Today* **2009**, *146*, 9–14.
100. Longoni, G.; Chini, P. Synthesis and chemical characterization of platinum carbonyl dianions  $[\text{Pt}_3(\text{CO})_6]_n^{2-}$  ( $n = \text{apprx.} 10, 6, 5, 4, 3, 2, 1$ ). A new series of inorganic oligomers. *J. Am. Chem. Soc.* **1976**, *98*, 7225–7231.
101. Holade, Y.; Morais, C.; Servat, K.; Napporn, T.W.; Kokoh, K.B. Toward the Electrochemical Valorization of Glycerol: Fourier Transform Infrared Spectroscopic and Chromatographic Studies. *ACS Catal.* **2013**, *3*, 2403–2411.
102. Holade, Y.; MacVittie, K.; Conlon, T.; Guz, N.; Servat, K.; Napporn, T.W.; Kokoh, K.B.; Katz, E. Pacemaker Activated by an Abiotic Biofuel Cell Operated in Human Serum Solution. *Electroanalysis* **2014**, *26*, 2445–2457.
103. Holade, Y.; Engel, A.B.; Tingry, S.; Servat, K.; Napporn, T.W.; Kokoh, K.B. Insights on Hybrid Glucose Biofuel Cell Based on Bilirubin Oxidase Cathode and Gold-Based Nanomaterials Anode. *ChemElectroChem* **2014**, *1*, 1976–1987.
104. Lim, B.; Kobayashi, H.; Camargo, P.C.; Allard, L.; Liu, J.; Xia, Y. New insights into the growth mechanism and surface structure of palladium nanocrystals. *Nano Res.* **2010**, *3*, 180–188.
105. Zhang, H.; Jin, M.; Xiong, Y.; Lim, B.; Xia, Y. Shape-Controlled Synthesis of Pd Nanocrystals and Their Catalytic Applications. *Acc. Chem. Res.* **2013**, *46*, 1783–1794.
106. Langille, M.R.; Personick, M.L.; Zhang, J.; Mirkin, C.A. Defining Rules for the Shape Evolution of Gold Nanoparticles. *J. Am. Chem. Soc.* **2012**, *134*, 14542–14554.
107. Huang, X.; Li, Y.; Li, Y.; Zhou, H.; Duan, X.; Huang, Y. Synthesis of PtPd Bimetal Nanocrystals with Controllable Shape, Composition, and Their Tunable Catalytic Properties. *Nano Lett.* **2012**, *12*, 4265–4270.
108. Holade, Y.; Servat, K.; Napporn, T.W.; Kokoh, K.B. Electrocatalytic properties of nanomaterials synthesized from “Bromide Anion Exchange” method—Investigations of glucose and glycerol oxidation. *Electrochim. Acta* **2015**, doi:10.1016/j.electacta.2014.11.072.
109. Habrioux, A.; Servat, K.; Tingry, S.; Kokoh, K.B. Enhancement of the performances of a single concentric glucose/O<sub>2</sub> biofuel cell by combination of bilirubin oxidase/Nafion cathode and Au–Pt anode. *Electrochem. Commun.* **2009**, *11*, 111–113.
110. Lee, W.-D.; Lim, D.-H.; Chun, H.-J.; Lee, H.-I. Preparation of Pt nanoparticles on carbon support using modified polyol reduction for low-temperature fuel cells. *Int. J. Hydrogen Energy* **2012**, *37*, 12629–12638.
111. Sakai, G.; Arai, T.; Matsumoto, T.; Ogawa, T.; Yamada, M.; Sekizawa, K.; Taniguchi, T. Electrochemical and ESR Study on Pt-TiO<sub>2</sub>/C Electrocatalysts with Enhanced Activity for ORR. *ChemElectroChem* **2014**, *1*, 366–370.
112. Teranishi, T.; Kurita, R.; Miyake, M. Shape Control of Pt Nanoparticles. *J. Inorg. Organomet. Polym.* **2000**, *10*, 145–156.

113. Mirdamadi-Esfahani, M.; Mostafavi, M.; Keita, B.; Nadjó, L.; Kooyman, P.; Remita, H. Bimetallic Au-Pt nanoparticles synthesized by radiolysis: Application in electro-catalysis. *Gold Bull.* **2010**, *43*, 49–56.
114. Rivadulla, J.F.; Vergara, M.C.; Blanco, M.C.; López-Quintela, M.A.; Rivas, J. Optical Properties of Platinum Particles Synthesized in Microemulsions. *J. Phys. Chem. B* **1997**, *101*, 8997–9004.
115. Lim, B.; Jiang, M.; Tao, J.; Camargo, P.H.C.; Zhu, Y.; Xia, Y. Shape-Controlled Synthesis of Pd Nanocrystals in Aqueous Solutions. *Adv. Funct. Mater.* **2009**, *19*, 189–200.
116. Wang, Z.-L.; Yan, J.-M.; Wang, H.-L.; Ping, Y.; Jiang, Q. Pd/C Synthesized with Citric Acid: An Efficient Catalyst for Hydrogen Generation from Formic Acid/Sodium Formate. *Sci. Rep.* **2012**, *2*, 598.
117. Klotz, P.; Feldberg, S.; Newman, L. Mixed-ligand complexes of palladium(II) with bromide and chloride in acetonitrile. *Inorg. Chem.* **1973**, *12*, 164–168.
118. Ksar, F.; Ramos, L.; Keita, B.; Nadjó, L.; Beaunier, P.; Remita, H. Bimetallic Palladium–Gold Nanostructures: Application in Ethanol Oxidation. *Chem. Mater.* **2009**, *21*, 3677–3683.
119. Imbeault, R.; Reyter, D.; Garbarino, S.; Roué, L.; Guay, D. Metastable Au<sub>x</sub>Rh<sub>100-x</sub> Thin Films Prepared by Pulsed Laser Deposition for the Electrooxidation of Methanol. *J. Phys. Chem. C* **2012**, *116*, 5262–5269.
120. Bonneman, H.; Brijoux, W.; Brinkmann, R.; Fretzen, R.; Jousen, T.; Koppler, R.; Korall, B.; Neiteler, P.; Richter, J. Preparation, characterization, and application of fine metal particles and metal colloids using hydrotriorganoborates. *J. Mol. Catal.* **1994**, *86*, 129–177.
121. Bönemann, H.; Braun, G.A. Enantioselective Hydrogenations on Platinum Colloids. *Angew. Chem. Int. Ed.* **1996**, *35*, 1992–1995.
122. Choudhury, N.A.; Raman, R.K.; Sampath, S.; Shukla, A.K. An alkaline direct borohydride fuel cell with hydrogen peroxide as oxidant. *J. Power Sources* **2005**, *143*, 1–8.
123. Ma, J.; Choudhury, N.A.; Sahai, Y. A comprehensive review of direct borohydride fuel cells. *Renew. Sustain. Energy Rev.* **2010**, *14*, 183–199.
124. Wroblowa, H.S.; Yen Chi, P.; Razumney, G. Electroreduction of oxygen: A new mechanistic criterion. *J. Electroanal. Chem. Interf. Electrochem.* **1976**, *69*, 195–201.
125. Acres, G.J.K.; Frost, J.C.; Hards, G.A.; Potter, R.J.; Ralph, T.R.; Thompsett, D.; Burstein, G.T.; Hutchings, G.J. Electrocatalysts for fuel cells. *Catal. Today* **1997**, *38*, 393–400.
126. Xing, W.; Yin, G.; Zhang, J. *Rotating Electrode Methods and Oxygen Reduction Electrocatalysts*, 1st ed.; Elsevier: Amsterdam, The Netherlands, 2014; p. 322.
127. Srinivasan, S.; Ticianelli, E.A.; Derouin, C.R.; Redondo, A. Advances in solid polymer electrolyte fuel cell technology with low platinum loading electrodes. *J. Power Sources* **1988**, *22*, 359–375.
128. Wilson, M.S.; Valerio, J.A.; Gottesfeld, S. Low platinum loading electrodes for polymer electrolyte fuel cells fabricated using thermoplastic ionomers. *Electrochim. Acta* **1995**, *40*, 355–363.
129. Gloaguen, F.; Andolfatto, F.; Durand, R.; Ozil, P. Kinetic study of electrochemical reactions at catalyst-recast ionomer interfaces from thin active layer modelling. *J. Appl. Electrochem.* **1994**, *24*, 863–869.

130. Coutanceau, C.; Croissant, M.J.; Napporn, T.; Lamy, C. Electrocatalytic reduction of dioxygen at platinum particles dispersed in a polyaniline film. *Electrochim. Acta* **2000**, *46*, 579–588.
131. Li, B.; Amiruddin, S.; Prakash, J. A Kinetic Study of Oxygen Reduction Reaction on Palladium-Nickel Alloy Surfaces. *ECS Trans.* **2008**, *6*, 139–144.
132. Oh, H.-S.; Oh, J.-G.; Kim, H. Modification of polyol process for synthesis of highly platinum loaded platinum–carbon catalysts for fuel cells. *J. Power Sources* **2008**, *183*, 600–603.
133. Lebègue, E.; Baranton, S.; Coutanceau, C. Polyol synthesis of nanosized Pt/C electrocatalysts assisted by pulse microwave activation. *J. Power Sources* **2011**, *196*, 920–927.
134. Brunel, L.; Denele, J.; Servat, K.; Kokoh, K.B.; Jolival, C.; Innocent, C.; Cretin, M.; Rolland, M.; Tingry, S. Oxygen transport through laccase biocathodes for a membrane-less glucose/O<sub>2</sub> biofuel cell. *Electrochem. Commun.* **2007**, *9*, 331–336.
135. Silvert, P.Y.; Tekaia-Elhsissen, K. Synthesis of monodisperse submicronic gold particles by the polyol process. *Solid State Ionics* **1995**, *82*, 53–60.
136. Joseyphus, R.J.; Kodama, D.; Matsumoto, T.; Sato, Y.; Jeyadevan, B.; Tohji, K. Role of polyol in the synthesis of Fe particles. *J. Magn. Magn. Mater.* **2007**, *310*, 2393–2395.
137. Couto, G.G.; Klein, J.J.; Schreiner, W.H.; Mosca, D.H.; de Oliveira, A.J. A.; Zarbin, A.J.G. Nickel nanoparticles obtained by a modified polyol process: Synthesis, characterization, and magnetic properties. *J. Colloid Int. Sci.* **2007**, *311*, 461–468.
138. Tzitzios, V.; Basina, G.; Gjoka, M.; Alexandrakis, V.; Georgakilas, V.; Niarchos, D.; Boukos, N.; Petridis, D. Chemical synthesis and characterization of hcp Ni nanoparticles. *Nanotechnology* **2006**, *17*, 3750–3755.
139. Kalyan Kamal, S.S.; Sahoo, P.K.; Premkumar, M.; Rama Rao, N.V.; Jagadeesh Kumar, T.; Sreedhar, B.; Singh, A.K.; Ram, S.; Chandra Sekhar, K. Synthesis of cobalt nanoparticles by a modified polyol process using cobalt hydrazine complex. *J. Alloys Compd.* **2009**, *474*, 214–218.
140. Ducamp-Sanguesa, C.; Herrera-Urbina, R.; Figlarz, M. Synthesis and characterization of fine and monodisperse silver particles of uniform shape. *J. Solid State Chem.* **1992**, *100*, 272–280.
141. Donati, I.; Travan, A.; Pelillo, C.; Scarpa, T.; Coslovi, A.; Bonifacio, A.; Sergio, V.; Paoletti, S. Polyol Synthesis of Silver Nanoparticles: Mechanism of Reduction by Alditol Bearing Polysaccharides. *Biomacromolecules* **2009**, *10*, 210–213.
142. Blosi, M.; Albonetti, S.; Dondi, M.; Martelli, C.; Baldi, G. Microwave-assisted polyol synthesis of Cu nanoparticles. *J. Nanopart. Res.* **2011**, *13*, 127–138.
143. Cuya Huaman, J.L.; Sato, K.; Kurita, S.; Matsumoto, T.; Jeyadevan, B. Copper nanoparticles synthesized by hydroxyl ion assisted alcohol reduction for conducting ink. *J. Mater. Chem.* **2011**, *21*, 7062–7069.
144. Jo, Y.H.; Jung, I.; Choi, C.S.; Kim, I.; Lee, H.M. Synthesis and characterization of low temperature Sn nanoparticles for the fabrication of highly conductive ink. *Nanotechnology* **2011**, *22*, 225701.
145. Nørskov, J.K.; Rossmeisl, J.; Logadottir, A.; Lindqvist, L.; Kitchin, J.R.; Bligaard, T.; Jónsson, H. Origin of the Overpotential for Oxygen Reduction at a Fuel-Cell Cathode. *J. Phys. Chem. B* **2004**, *108*, 17886–17892.
146. Toda, T.; Igarashi, H.; Uchida, H.; Watanabe, M. Enhancement of the Electroreduction of Oxygen on Pt Alloys with Fe, Ni, and Co. *J. Electrochem. Soc.* **1999**, *146*, 3750–3756.

147. Xiong, L.; Manthiram, A. Effect of Atomic Ordering on the Catalytic Activity of Carbon Supported PtM (M = Fe, Co, Ni, and Cu) Alloys for Oxygen Reduction in PEMFCs. *J. Electrochem. Soc.* **2005**, *152*, A697–A703.
148. Yang, H.; Vogel, W.; Lamy, C.; Alonso-Vante, N. Structure and Electrocatalytic Activity of Carbon-Supported Pt–Ni Alloy Nanoparticles Toward the Oxygen Reduction Reaction. *J. Phys. Chem. B* **2004**, *108*, 11024–11034.
149. Santiago, E.I.; Varanda, L.C.; Villullas, H.M. Carbon-Supported Pt–Co Catalysts Prepared by a Modified Polyol Process as Cathodes for PEM Fuel Cells. *J. Phys. Chem. C* **2007**, *111*, 3146–3151.
150. Rao, C.V.; Reddy, A.L.M.; Ishikawa, Y.; Ajayan, P.M. Synthesis and electrocatalytic oxygen reduction activity of graphene-supported Pt<sub>3</sub>Co and Pt<sub>3</sub>Cr alloy nanoparticles. *Carbon* **2011**, *49*, 931–936.
151. Liu, C.; Wu, X.; Klemmer, T.; Shukla, N.; Yang, X.; Weller, D.; Roy, A.G.; Tanase, M.; Laughlin, D. Polyol Process Synthesis of Monodispersed FePt Nanoparticles. *J. Phys. Chem. B* **2004**, *108*, 6121–6123.
152. Venkateswara Rao, C.; Viswanathan, B. ORR Activity and Direct Ethanol Fuel Cell Performance of Carbon-Supported Pt–M (M = Fe, Co, and Cr) Alloys Prepared by Polyol Reduction Method. *J. Phys. Chem. C* **2009**, *113*, 18907–18913.
153. Min, M.-k.; Cho, J.; Cho, K.; Kim, H. Particle size and alloying effects of Pt-based alloy catalysts for fuel cell applications. *Electrochim. Acta* **2000**, *45*, 4211–4217.
154. Léger, J.M. Preparation and activity of mono- or bi-metallic nanoparticles for electrocatalytic reactions. *Electrochim. Acta* **2005**, *50*, 3123–3129.
155. Tseng, C.-J.; Lo, S.-T.; Lo, S.-C.; Chu, P.P. Characterization of Pt–Cu binary catalysts for oxygen reduction for fuel cell applications. *Mater. Chem. Phys.* **2006**, *100*, 385–390.
156. Xiong, L.; Kannan, A.M.; Manthiram, A. Pt–M (M = Fe, Co, Ni and Cu) electrocatalysts synthesized by an aqueous route for proton exchange membrane fuel cells. *Electrochem. Commun.* **2002**, *4*, 898–903.
157. Cambanis, G.; Chadwick, D. Platinum–vanadium carbon supported catalysts for fuel cell applications. *Appl. Catal.* **1986**, *25*, 191–198.
158. Antolini, E.; Passos, R.R.; Ticianelli, E.A. Electrocatalysis of oxygen reduction on a carbon supported platinum–vanadium alloy in polymer electrolyte fuel cells. *Electrochim. Acta* **2002**, *48*, 263–270.
159. Mukerjee, S.; Srinivasan, S.; Soriaga, M.P.; McBreen, J. Effect of Preparation Conditions of Pt Alloys on Their Electronic, Structural, and Electrocatalytic Activities for Oxygen Reduction—XRD, XAS, and Electrochemical Studies. *J. Phys. Chem.* **1995**, *99*, 4577–4589.
160. Huang, M.; Li, L.; Guo, Y. Microwave heated polyol synthesis of Pt<sub>3</sub>Te/C catalysts. *Electrochim. Acta* **2009**, *54*, 3303–3308.
161. Chen, C.; Kang, Y.; Huo, Z.; Zhu, Z.; Huang, W.; Xin, H.L.; Snyder, J.D.; Li, D.; Herron, J.A.; Mavrikakis, M.; *et al.* Highly crystalline multimetallic nanoframes with three-dimensional electrocatalytic surfaces. *Science* **2014**, *343*, 1339–1343.

162. Senthil Kumar, S.M.; Soler Herrero, J.; Irusta, S.; Scott, K. The effect of pretreatment of Vulcan XC-72R carbon on morphology and electrochemical oxygen reduction kinetics of supported Pd nano-particle in acidic electrolyte. *J. Electroanal. Chem.* **2010**, *647*, 211–221.
163. Murthi, V.S.; Urian, R.C.; Mukerjee, S. Oxygen Reduction Kinetics in Low and Medium Temperature Acid Environment: Correlation of Water Activation and Surface Properties in Supported Pt and Pt Alloy Electrocatalysts. *J. Phys. Chem. B* **2004**, *108*, 11011–11023.
164. Jiang, L.; Hsu, A.; Chu, D.; Chen, R. Oxygen Reduction Reaction on Carbon Supported Pt and Pd in Alkaline Solutions. *J. Electrochem. Soc.* **2009**, *156*, B370–B376.
165. Gasteiger, H.A.; Kocha, S.S.; Sompalli, B.; Wagner, F.T. Activity benchmarks and requirements for Pt, Pt-alloy, and non-Pt oxygen reduction catalysts for PEMFCs. *Appl. Catal. B* **2005**, *56*, 9–35.
166. Yam, V.W.W. Behind platinum's sparkle. *Nat. Chem.* **2010**, *2*, 790.
167. Borup, R.; Meyers, J.; Pivovar, B.; Kim, Y.S.; Mukundan, R.; Garland, N.; Myers, D.; Wilson, M.; Garzon, F.; Wood, D.; *et al.* Scientific Aspects of Polymer Electrolyte Fuel Cell Durability and Degradation. *Chem. Rev.* **2007**, *107*, 3904–3951.
168. Martins, C.; Fernández, P.; Troiani, H.; Martins, M.; Arenillas, A.; Camara, G. Agglomeration and Cleaning of Carbon Supported Palladium Nanoparticles in Electrochemical Environment. *Electrocatalysis* **2014**, *5*, 204–212.
169. Hiraoka, F.; Matsuzawa, K.; Mitsushima, S. Degradation of Pt/C Under Various Potential Cycling Patterns. *Electrocatalysis* **2013**, *4*, 10–16.
170. Cui, C.-H.; Yu, S.-H. Engineering Interface and Surface of Noble Metal Nanoparticle Nanotubes toward Enhanced Catalytic Activity for Fuel Cell Applications. *Acc. Chem. Res.* **2013**, *46*, 1427–1437.
171. Ma, J.; Habrioux, A.; Alonso-Vante, N. The Effect of Substrates at Cathodes in Low-temperature Fuel Cells. *ChemElectroChem* **2014**, *1*, 37–46.
172. Jiang, Z.-Z.; Wang, Z.-B.; Chu, Y.-Y.; Gu, D.-M.; Yin, G.-P. Ultrahigh stable carbon riveted Pt/TiO<sub>2</sub>-C catalyst prepared by *in situ* carbonized glucose for proton exchange membrane fuel cell. *Energy Environ. Sci.* **2011**, *4*, 728–735.
173. Strmcnik, D.; Kodama, K.; van der Vliet, D.; Greeley, J.; Stamenkovic, V.R.; Marković, N.M. The role of non-covalent interactions in electrocatalytic fuel-cell reactions on platinum. *Nat. Chem.* **2009**, *1*, 466–472.
174. Strmcnik, D.; Escudero-Escribano, M.; Kodama, K.; Stamenkovic, V.R.; Cuesta, A.; Marković, N.M. Enhanced electrocatalysis of the oxygen reduction reaction based on patterning of platinum surfaces with cyanide. *Nat. Chem.* **2010**, *2*, 880–885.
175. Zhang, J.; Sasaki, K.; Sutter, E.; Adzic, R.R. Stabilization of Platinum Oxygen-Reduction Electrocatalysts Using Gold Clusters. *Science* **2007**, *315*, 220–222.
176. Sepa, D.B.; Vojnovic, M.V.; Vracar, L.M.; Damjanovic, A. Apparent enthalpies of activation of electrodic oxygen reduction at platinum in different current density regions—I. Acid solution. *Electrochim. Acta* **1986**, *31*, 91–96.
177. Damjanovic, A. Electron transfer through thin anodic films in oxygen evolution at Pt electrodes in alkaline solutions. *Electrochim. Acta* **1992**, *37*, 2533–2539.

178. Demarconnay, L.; Coutanceau, C.; Léger, J.M. Electroreduction of dioxygen (ORR) in alkaline medium on Ag/C and Pt/C nanostructured catalysts—effect of the presence of methanol. *Electrochim. Acta* **2004**, *49*, 4513–4521.

© 2015 by the authors; licensee MDPI, Basel, Switzerland. This article is an open access article distributed under the terms and conditions of the Creative Commons Attribution license (<http://creativecommons.org/licenses/by/4.0/>).